Source apportionment resolved by time-of-day for improved deconvolution of primary source contributions to air pollution

Sahil Bhandari[1], Zainab Arub[2], Gazala Habib[2], Joshua S. Apte[3,4], and Lea Hildebrandt Ruiz[5]

[1]Department of Mechanical Engineering, University of British Columbia, Vancouver, Canada
5 [2]Department of Civil Engineering, Indian Institute of Technology Delhi, New Delhi, India
[3]Department of Civil and Environmental Engineering, UC Berkeley, California, USA
[4]School of Public Health, UC Berkeley, California, USA
[5]McKetta Department of Chemical Engineering, The University of Texas at Austin, Texas, USA

Correspondence to: Lea Hildebrandt Ruiz (lhr@che.utexas.edu) and Joshua S. Apte (apte@berkeley.edu)

10 **Abstract.** Present methodologies for source apportionment assume fixed source profiles. Since meteorology and human activity patterns change seasonally and diurnally, application of source apportionment techniques to shorter rather than longer time periods generates more representative mass spectra. Here, we present a new method to conduct source apportionment resolved by time of day using the underlying approach of positive matrix factorization (PMF). We call this approach "time-of-day PMF" and statistically demonstrate the improvements in this approach over traditional PMF. We report on source
15 apportionment conducted on four example time periods in two seasons (winter and monsoon 2017), using organic aerosol measurements from an Aerosol Chemical Speciation Monitor (ACSM). We deploy the EPA PMF tool with the underlying Multilinear Engine (ME-2) as the PMF solver. Compared to the traditional seasonal PMF approach, we extract a larger number of factors as well as PMF factors that represent the expected sources of primary organic aerosol using time-of-day PMF. By capturing diurnal time series patterns of sources at a low computational cost, time-of-day PMF can utilize large datasets
20 collected using long-term monitoring and improve the characterization of sources of organic aerosol compared to traditional PMF approaches that do not resolve by time of day.

1 Introduction

Air pollution is considered the greatest current environmental health threat to humanity, with an estimated mortality burden of 7 million per year (World Health Organization, 2018; Schraufnagel et al., 2019; Health Effects Institute, 2020). Air pollutants
25 also cause climate forcing and environmental damages to ecosystems and biodiversity (Intergovernmental Panel on Climate Change, 2019; Intergovernmental Panel on Climate Change, 2021). Apart from physiological and environmental effects, air pollution is associated with negative psychological, economic, and social effects (Lu et al., 2020). High racial, ethnic, income, regional, and nationality-based disparities exist in air pollution exposure, making air pollution exposure an important environmental justice issue (Hajat et al., 2015; Goodkind et al., 2019; Tessum et al., 2019; Thind et al., 2019; Health Effects
30 Institute, 2020; Pandey et al., 2020; Chakraborty et al., 2021). These disparities are associated with a wide variety of sectors,

activities, processes, and pollutants (Thakrar et al., 2020). Policy solutions targeting specific pollutants have led to non-uniform reductions of air pollution contributions of different sectors (Tschofen et al., 2019). Thus, reduction of air pollution is essential to global health and can be expected to generate long-term societal benefits (Tessum et al., 2018; Tschofen et al., 2019; Organization for Economic Co-operation and Development, 2020). However, more than half the world's population is exposed

35 to increasing air pollution (Shaddick et al., 2020). Most of this population lives in developing nations. Moreover, economic resources are limited, and reduction of air pollution alongside continued economic growth requires investment in abatement measures for older technologies and adoption of cleaner technologies (Lei et al., 2021). Thus, sources of air pollution need to be prioritized to appropriately focus limited resources on the most effective abatement measures. This prioritization should be based on the contributions of different emission sources to air pollution in a region.

40 Source apportionment is the practice of attributing air pollution to different causes such as sectors (residential, industrial), activities (traffic, biomass burning) and atmospheric processes (oxidation). Several approaches have been developed to conduct source apportionment studies (Belis et al., 2014). Broadly, these approaches can be categorized into emission inventories, receptor-oriented modeling, and source-oriented modeling. These approaches have been accepted by regional, national, and international agencies for use in air quality policy and planning (Belis et al., 2014; Environmental

45 Protection Agency, 2017; California Air Resources Board, 2018; Wayland, 2018). Source-oriented models and emission inventories together capture the emissions, chemical transformation, transport, and dispersion of pollution. However, they have heavy computational burden, require extensive data collection, and are subject to cumulative uncertainties from model inputs as well as the different computational components (Hopke et al., 2016). Receptor models are mathematical tools with relatively lower computational requirements that use mass balance analysis to output source contributions (time series of source

50 concentrations) and source profiles (relative strength of different pollutants) for identified sources of air pollution (Belis et al., 2013; Hopke et al., 2016). Positive Matrix Factorization (PMF) has been identified as an appropriate receptor modeling technique that can be deployed for quantifying source contributions for air quality management (Belis et al., 2015).

Three tools are currently in active use for application of PMF to atmospheric datasets: the IGOR PMF Evaluation Tool (PET) (Ulbrich et al., 2009), the EPA PMF tool (Brown et al., 2012), and Source Finder (SoFi) (Canonaco et al., 2013).

55 The IGOR PET tool uses the PMF2 program to resolve factors from 2-D matrices (Paatero and Tapper, 1994; Ulbrich et al., 2009). Further details on the statistical basis of this method are available elsewhere (Ulbrich et al., 2009; Zhang et al., 2011, and references therein). Both SoFi and EPA PMF are based on the Multilinear Engine (ME-2), which allows the application of factor profile constraints to extract specific sources (Paatero et al., 1999; Paatero et al., 2002; Canonaco et al., 2013; Crippa et al., 2014; Norris et al., 2014). PMF2 does not allow the application of factor profile constraints, and it often results in greater

60 uncertainty in solutions, poorer source separation, and fewer identified sources compared to ME-2 (Ramadan et al., 2003, Amato et al., 2009; Amato and Hopke, 2012). A further important advantage of the EPA PMF tool over Igor PET and SoFi are its error estimation techniques, which systematically account for both random error and rotational ambiguity using bootstrapping, displacements, and bootstrap-displacements, as explained in more detail in Sect. 2.5. (Paatero et al., 2014;

2

Brown et al., 2015). Currently, the IGOR PET and the SoFi tools only use bootstrapping to account for random errors and,
65 partially, rotational ambiguity (Ulbrich et al., 2009; Canonaco et al., 2020).

PMF tools have been applied to identify sources using long-term datasets spanning multiple years (Zhang et al., 2019; Heikkinen et al., 2020), seasonal datasets accounting for seasonal variability (Amil et al., 2016; Bikkina et al., 2019; Bhandari et al., 2020; Patel et al., 2021a), for studying special events (Reyes-Villegas et al., 2018; Rai et al., 2020, Patel et al., 2021b), to study spatial variability (Crippa et al., 2014; Robinson et al., 2018), as well as to connect sources to health effects
70 (Daellenbach et al., 2020). Several studies have analysed the influence of meteorology after conducting source apportionment on a larger dataset (Venturini et al., 2014; Pauraite et al., 2019; Bhandari et al., 2020). Some studies have quantified the effect of meteorological variables on the performance of the source apportionment approach for the identification of sources, with or without stratification. One such study stratified data based on mean temperature and showed that accounting for temperature variability using gas-particle partitioning before conducting source apportionment improved the stability of the solution (Xie
75 et al., 2013a, b). Similar data-segmentation schemes have been deployed for wind direction, wind speed, and precipitation, and these techniques resulted in a larger and more representative PMF factors (Park et al., 2019).

A major limitation of PMF is the assumption of constant factor profiles throughout the modeling period—while the contribution of each factor is modelled to change over time, its profile (e.g., mass spectrum, when PMF is applied to mass spectrometer data) stays constant, which leads to modeling uncertainty (Ulbrich et al., 2009). Previous studies have tested the
80 limitation of constant mass spectral profiles for seasonal and weekly changes in meteorology and activity patterns (Canonaco et al., 2015; Reyes-Villegas et al., 2016; Canonaco et al., 2020). These studies found that annual and seasonal datasets from an Aerosol Chemical Speciation Monitor (ACSM; Aerodyne Research, Billerica, MA) show high variations in mass spectral contributions which cannot be sufficiently captured when PMF is conducted on the complete dataset. These studies recommended conducting PMF analysis on shorter time frames (weeks–months) with limited variability of emissions and
85 meteorology. However, meteorological conditions influence source apportionment on hourly and smaller time scales; for example, changes in ventilation (Dai et al., 2020) and photochemistry (Lelieveld et al., 1991) affect source apportionment results. Human activity patterns also vary with time leading to changes in source cocktails—for example, we expect higher cooking emissions during cooking-influenced periods (Abdullahi et al., 2013; Patel et al., 2021), higher traffic emissions during rush hours (Zhang et al., 2013), and time-of-day, day-of-week, and month-of-year patterns for other emission sources (Crippa
90 et al., 2020). These changes in meteorology, photochemistry, and sources lead to diurnal variability in mass spectra. For example, Canonaco et al. (2015) showed that the mass spectra of secondary organic aerosol (SOA) changed with concentrations of OX (O_3+NO_2), which shows high diurnal variability due to monotonic association with ambient temperature. Finally, diurnal variability of time series patterns is frequently used for PMF factor selection and representation (Zhang et al., 2011). As an example, using data from 11 days of PMF runs, Williams et al. (2010) presented bihourly diurnal
95 variability of PMF factor time series contributions. Recognizing the importance of variability of source influence at receptor sites, previous research has examined the influence of sampling periods, sampling time resolution, and time series variability of source emissions on the final PMF result (Tian et al., 2017; Wang et al., 2018). Results from these studies suggest that,

given the assumption of constant factor profiles in PMF, PMF analysis should be conducted on time-resolved datasets. Additionally, to capture source emission and meteorological variability over the day, data from all times of day should be collected. Thus, an ideal PMF technique would make the most of the high-time resolution of datasets while assuming constant factor profiles for periods with limited variability in emissions and meteorology.

One such approach is conducting different PMF runs for different times of the day across long-term datasets. A key advantage of such sub-setting is that it captures the diurnal variability in source apportionment using PMF while keeping computational load to a minimum. Differences in factor profiles between the seasonal PMF and time-of-day PMF runs may indicate the effect of diurnal process changes and/or reactivity (Norris et al., 2014). Conducting PMF on smaller time windows is expected to improve results for another reason. Positive Matrix Factorization approaches have influence functions that are designed to account for the influence of outliers on the solutions (Paatero et al., 1994; Paatero et al., 1997; Ulbrich et al., 2009). These outliers depend on the time window on which the factorization is being applied (Paatero et al., 1997). A shorter time window for analysis is influenced by outliers present in that time window only, and not any other period. Thus, a shorter time window can be expected to give higher factor resolution, given that the influence of many outliers in the dataset is removed. At the same time, the number of zeros in the dataset also assists with the quantification of PMF factors (Paatero et al., 1997). Thus, shortening time windows can also decrease the extraction of factors via PMF, as has been reported previously (Tian et al., 2017).

This paper improves upon the seasonal source apportionment previously employed in Delhi (Bhandari et al., 2020). The Delhi Aerosol Supersite (DAS) study provides long-term chemical characterization of ambient submicron aerosol in Delhi, with near-continuous online measurements of aerosol composition (Gani et al., 2019; Arub et al., 2020; Bhandari et al., 2020; Gani et al., 2020; Patel et al., 2021a). In that study, PMF was conducted on six seasons of highly time-resolved speciated non-refractory submicron aerosol (NR-PM$_1$) organic (Org) mass spectrometer data from an Aerosol Chemical Speciation Monitor (ACSM) in the PMF receptor model at a time resolution of 5–6 min. Then, we deployed the IGOR PET tool on seasonal datasets and 2–3 PMF factors were extracted. The extraction of a low number of factors implies low rotations, and therefore quantitative error estimation was not conducted in that study (Paatero et al., 1994).

Here, we apply the approach of conducting PMF on long-term datasets where each day was separated into six 4 hour periods with limited variability in emissions and meteorology. In our knowledge, no study has systematically assessed the use of PMF on data resolved by time of day. In this paper, we report on PMF conducted on ACSM organic aerosol data from the two seasons of winter and monsoon 2017—collected as a part of the Delhi Aerosol Supersite (DAS) study—after resolving by time-of-day. Thus, factor MS is expected to vary in these time-of-day windows. The two seasons of winter and monsoon are selected for this analysis as they capture two extremes in seasonal concentrations, precipitation, and meteorology, especially in terms of temperature, ventilation coefficient, wind direction, and wind speed (Tables S1 and S2, Fig. S1). In addition, winter experiences extremely high organic and inorganic concentrations and high pollution episodes dominated by primary emissions (Gani et al., 2019; Bhandari et al., 2020). We use the EPA PMF tool to apply constraints, extract a larger number of factors, and quantify errors in PMF solutions.

2 Methods

2.1 Statistical basis of approach

ME-2 is a multilinear unmixing model that can be used to perform bilinear deconvolution of a measured mass spectral matrix ($\mathbf{X}$) into the product of positively constrained mass spectral profiles ($\mathbf{F}$) and their corresponding time series ($\mathbf{G}$), as shown in Eq. (1). In Eq. (1), $\mathbf{E}$ corresponds to the data residual not fit by the model. Given that time series and mass spectra are deconvoluted, the model mass spectral profiles are assumed to remain constant in time. The mass balance equation underlying the bilinear implementation of the factor analytical model and the optimization problem in the EPA PMF tool can be represented as shown in Eq. 1–3.

$$X = GF + E \tag{1}$$

$$x_{ij} = \sum_{p=1}^{n} g_{ip} \cdot f_{pj} + e_{ij} \tag{2}$$

Equation (2) is an elemental notation of Eq. (1). For ACSM data analysed here, x_{ij} represents an element of the $m \times n$ data matrix $\mathbf{X}$, where i represents a single time point and j represents a measured ion or m/z. n corresponds to the number of factors in the PMF solution. Thus, g_{ip} refers to the time series contribution of the pth factor at the ith time point, and f_{pj} represents the mass spectral contribution of the jth m/z in the pth factor profile.

To derive factor time series and mass spectra in an iterative fitting process, ME-2 lowers residual by minimizing the quality of fit parameter Q, using the gradient approach (Norris et al., 2014; Eq. (3)). Thus, PMF attempts to achieve a global minimum to the optimization problem. Q is the weighted least-squares error (sum of squares of model error normalized to measurement error), or the summation of squares of scaled residuals of the fit at each data point. We do not expect the norm of the actual error matrix to be zero but instead close to the ACSM measured uncertainty (an element of the measured uncertainty is represented as σ_{ij} in Eq. (3)). The quality of fit parameter corresponding to this uncertainty is called $Qexp$ (Ulbrich et al., 2009). While $Qexp$ is precisely equal to $mn-p(m+n)$, for large m, n, it simplifies to $\sim mn$. Usually, PMF solutions start from very high $Q/Qexp$, and converge to 1 as more factors are added. We refer to the Q for the entire dataset as $Q0$.

$$Q0 = Min_{F,G} Q = \sum_{i=1}^{m} \sum_{j=1}^{n} \left(e_{ij}/\sigma_{ij} \right)^2 \tag{3}$$

For this discussion, we assume that Eq. (3) is subject to a constant mass spectrum $F0$, and variable time series $G0$. A key limitation of PMF is that it assumes constant MS profiles, even though source signatures can change over the course of the day. To address this limitation, we divide our data into time segments to conduct PMF analysis resolved by time-of-day. We refer to this time-resolved organic MS-based PMF as "time-of-day PMF" and the traditional approach as "seasonal PMF" in the paper. In the time-of-day PMF approach presented here, we minimize Q separately in each of these time-of-day windows.

5

2.2 Mathematical formulation of the time-of-day PMF approach

The mathematical formulation of the time-of-day PMF approach is introduced in Eqs. 4–17. To provide an example for splitting of data by time-of-day, we modify Eq. 3, dividing the data matrix $\mathbf{X}$ into $\mathbf{X_{day}}$ (time, $t \in [12$ am, 12 pm$)$) and $\mathbf{X_{night}}$ (time, $t \in [12$ pm, 12 am$)$) (Eq. 4). Here, we demonstrate that splitting the data by time-of-day will result in a better solution. Thus,

$$X = \{X_{day}, X_{night}\} \tag{4}$$

The mathematical representation of the objective functions for conducting PMF separately for $\mathbf{X_{day}}$ and $\mathbf{X_{night}}$ periods are shown in Eq. 5 and Eq. 6 respectively. We call Q for these data subsets $Q1$ and $Q2$.

$$Q1 = Min_{F,G} \left(\sum_{i=1}^{m} \sum_{j=1 \ni time \in Xday}^{n} (e_{ij}/\sigma_{ij})^2 \right) \tag{5}$$

$$Q2 = Min_{F,G} \left(\sum_{i=1}^{m} \sum_{j=1 \ni time \in Xnight}^{n} (e_{ij}/\sigma_{ij})^2 \right) \tag{6}$$

For this discussion, we assume that Eq. (5) is subject to a constant mass spectrum $\mathbf{F1}$, and variable time series $\mathbf{G1}$ for dataset $\mathbf{X_{day}}$, and Eq. (6) is subject to a constant mass spectrum $\mathbf{F2}$, and variable time series $\mathbf{G2}$ for the dataset $\mathbf{X_{night}}$. For simplification,

$$A(F, G) = \sum_{i=1}^{m} \sum_{j=1 \ni time \in Xday}^{n} (e_{ij}/\sigma_{ij})^2 \tag{7}$$

$$B(F, G) = \sum_{i=1}^{m} \sum_{j=1 \ni time \in Xnight}^{n} (e_{ij}/\sigma_{ij})^2 \tag{8}$$

Thus,
$$Q1(F1, G1) = Min(A) \wedge Q2(F2, G2) = Min(B) \tag{9}$$

Using these definitions, we can also redefine $Q0$ as shown in Eq. 10.

$$Q0(F0, G0) = Min(A + B) \tag{10}$$

Clearly, $Q0$ minimizes the sum of two functions A and B. Thus, $Q0$ is a multi-objective optimization problem attempting to achieve global minimum for the combined dataset $\mathbf{X}$ (Gunantara et al., 2018; Eq. 10). The two functions A and B are globally minimized separately at ($\mathbf{F1}$, $\mathbf{G1}$) in Eq. 5 and at ($\mathbf{F2}$, $\mathbf{G2}$) in Eq. 6, respectively. Thus, by definition, Eq. 5 and Eq. 6 can be written as:

$$Min_{F,G} A \leq A \, for all (F, G) \tag{11}$$

$$Min_{F,G} B \leq B \, for all (F, G) \tag{12}$$

Adding the inequalities in Eq. (11) and Eq. (12), we get:

$$Min_{F,G}(A) + Min_{F,G}(B) \leq A + B \, for all (F, G) \tag{13}$$

Since this is true for all ($\mathbf{F}$, $\mathbf{G}$), this is also true for ($\mathbf{F}$, $\mathbf{G}$) that gives the minimum of $A + B$. Thus,

$$Min_{F,G}(A) + Min_{F,G}(B) \leq Min_{F,G}(A + B), \vee \tag{14}$$

$$Q1 + Q2 \leq Q0, \vee \tag{15}$$

$$Q1 + Q2 \leq Q0_1 + Q0_2 \tag{16}$$

In Eq. (16), $Q0_1$ and $Q0_2$ are Q contributions to $Q0$ in the ($\mathbf{F}$, $\mathbf{G}$) space corresponding to $Q1$ and $Q2$ respectively. Thus, we can see that if solutions to $Q0$ will attempt to minimize error in the ($\mathbf{F}$, $\mathbf{G}$) space corresponding to $Q1$ (minimize $Q0_1$), the obtained solution will likely worsen the error in the ($\mathbf{F}$, $\mathbf{G}$) space corresponding to $Q2$ (and therefore, not minimize $Q0_2$). This property of solutions to multi-objective optimization problems is inherent to a large class of solutions known as Pareto solutions, which

are used for source apportionment and air quality planning (Gunantara et al., 2018; Angelis et al., 2020). This limitation can also be viewed as a limitation on the mass spectral profiles—*Q0* assumes constant mass spectral profiles for both day and night periods, and likely fits both periods worse than the scenarios of *Q1* and *Q2*, where separate mass profiles for the two periods were developed. Thus, in the traditional approach, varying TS on non-varying MS can only capture changes as a linear TS scaling factor for all MS contributions. In the time-of-day PMF approach, both MS and TS are varying, and we can expect new MS and TS patterns. For the special case of day-night data split, where equal number of points are collected in X_{day} and X_{night}, *Qexp (~ mn)* corresponding to the two matrices are equal (we call it *Qexp$_{dn}$*), whereas we call it *Qexp* corresponding to the matrix **X** would be double that value (*2Qexp$_{dn}$*). Using these *Qexp$_{dn}$* values, Eq. 16 can be written as

$$Q1/Qexp_{dn} + Q2/Qexp_{dn} \leq Q0_1/Qexp_{dn} + Q0_2/Qexp_{dn} \qquad (17)$$

Clearly, using the day-night split thought experiment, we show that the sum of *Q1* and *Q2* (and the equivalent sum in *Q/Qexp*) would be lower than *Q0* (and the equivalent sum of *Q/Qexp* components). By inference, dividing the time series into periods of similar length (six 4 hour segments in this manuscript) should result in a similar relationship as Eq. (17). Overall, conducting PMF on each of such time-of-day periods challenges the assumption of diurnally non-varying MS factors in typical PMF.

Table 1 Summary of meteorology in the time-of-day PMF periods

Season and Period	T (K)	RH (%)	VC[a] (m²/s)	PBLH* (m)	WS (m/s)	WD (°N)	Nomenclature
W17 1100–1500 LT	294	93	3870 (3790)	1353 (1356)	2.9	-14.0	W-11-15
W17 2300–0300 LT	286	62	707 (188)	273 (64)	2.5	-49.0	W-23-03
M17 1100–1500 LT	308	82	6179 (6222)	2022 (2061)	3.1	6.9	M-11-15
M17 2300–0300 LT	302	73	1182 (237)	428 (84)	2.5	68.0	M-23-03

[a]Median values for VC and PBLH are reported in parenthesis.

2.3 Sampling site and measurements

As a part of the DAS study, an ACSM (Aerodyne Research, Billerica, MA) was operated at ~0.1 L min^{-1} at ~1 min time resolution in a temperature-controlled laboratory on the top floor of a four-story building at IIT Delhi (Ng et al., 2011b). Additionally, BC, ultraviolet-absorbing particulate matter (UVPM), and their difference ΔC were measured using a seven-wavelength aethalometer operated at the 1L min^{-1} flow rate and 1 min time resolution (Magee Scientific Model AE33, Berkeley, CA) (Drinovec et al., 2015). These instruments were on separate sampling lines, both of which had a PM$_{2.5}$ cyclone followed by a water trap and a Nafion membrane diffusion dryer (Magee Scientific sample stream dryer, Berkeley, CA). Full details of sampling site, instrument setup, operating procedures, calibrations, and data processing are described in a separate publication (Gani et al., 2019).

We collected the data used in this paper in winter (January–February 2017) and monsoon (July–September 2017). Definition of the seasons comes from the Indian National Science Academy (2018) (Table 2 from Bhandari et al., 2020).

220 Diurnal plots of meteorological variables are shown in Fig. S1. We conduct seasonal PMF runs for winter and monsoon 2017 and time-of-day PMF runs for two periods (1100–1500 LT and 1900–2300 LT) in the two seasons. We used the dataset obtained by averaging every five consecutive measurements for the seasonal PMF runs. We selected organic spectral data at a specific set of m/z values between m/z 12 and m/z 120. This approach is the commonly used approach, and the reasons for the selection of the specific set of m/z values have been described previously (Zhang et al., 2005). Spring, summer, and autumn

225 (mid-September to November) periods are not included in the analysis here; but seasonal PMF analysis has been presented in previous publications (Bhandari et al., 2020; Patel et al., 2021a).

2.4 PMF tool and runs

Here, we used two alternative approaches for conducting PMF. In one approach, we apply PMF by splitting the data into six 4 hour time windows each day to illustrate the use of our time-of-day PMF method. The choice of the four-hour window was

230 based on a preliminary PMF analysis conducted on monsoon that allowed us to identify the influence of cooking organic aerosol, based on the ratio of contributions at m/z 55:57 (Robinson et al, 2018). We started from 12 hour time windows and kept decreasing the window size until the ratio was substantially greater than 1.6, suggesting the presence of a COA factor in at least one such time window (in this case, it was M-23-03, Table 2). We also conduct seasonal PMF runs for winter and monsoon 2017 and time-of-day PMF runs for two periods (1100–1500 LT-local time and 1900–2300 LT) in the two seasons.

235 Thus, we conduct four time-of-day PMF runs in total. The two time-of-day periods in each season are selected to differentiate between the influence of primary sources, changing MS due to reaction chemistry, and the effect of meteorology (Table 1, Fig. S1). As shown in the companion paper, these periods represent the two extremes in total $NRPM_1$ concentrations (Tables 1–2, Bhandari et al., 2022). Results from PMF analysis for all times of the day are presented in a companion paper (Bhandari et al., 2022), and a brief summary of those results is also provided in the Supplement of this paper (Sect. S5). In monsoon and winter,

240 traffic is expected to be a dominant source at night due to low cooking-related emissions and overlap with high nighttime traffic on major traffic corridors (Mishra et al., 2019). At midday in monsoon, high temperatures and solar flux imply high photochemical processing of aerosols; therefore, we expect to see more oxidized aerosols (Table 1, Fig. S1). At winter nighttime, biomass burning for heating is an expected source. To refer to PMF runs corresponding to specific time windows, we use the nomenclature "Season" + "Period" style in the format "S-TT-TT" (Table 1). For example, W-11-15 corresponds to

245 the 1100–1500 LT of Winter 2017. Using data presented in this paper, we also compare the Q (and Q/Qexp) values from the seasonal PMF runs corresponding to the periods of the time-of-day windows (Sect. 3.5). While this work addresses the diurnal variations in MS patterns, future work could investigate the optimal length of the time window to sufficiently represent the finer diurnal variations (less than four hours) in mass spectral profiles while managing computational burden.

The EPA PMF v5.0 tool was used to conduct ME-2 analysis on this dataset and interpret its results (Norris et al.,

250 2014). Further details on the statistical basis of this method are available elsewhere (Paatero et al., 1999; Paatero et al., 2002). For the base run, the iterative PMF technique does not make any assumptions for source or time profiles. If factors extracted in the base run were not clearly associated with a source type but suggestive of the presence or mixing of specific sources,

constraints were applied on the factors in the base run to extract cleaner source profiles (Brown et al., 2012; Brown et al., 2015). An R package was developed to automate the process of data analysis of EPA PMF outputs (R Core Team, 2019). We readjusted the results from PMF analysis to account for underestimation of factor mass based on the selected m/z values only. To account for particle losses, we applied transmission and collection efficiencies after conducting PMF analysis (Gani et al., 2019).

Details of the steps for conducting PMF, R code, and criteria for factor selection are discussed in detail in the Supplement (Sect. S1). Briefly, for selection of PMF solutions, we started by analysing the different statistics of $Q/Qexp$ (a measure of fit), correlogram of residual TS and correlation with external tracers, time series patterns in residuals, and PMF fits at different m/zs (Table S4). We also considered the correlation of factor mass spectral profiles with reference mass spectra since MS of different factors are characterized by different spectral signature peaks (Zhang et al., 2011). For example, hydrocarbon-like organic aerosol (HOA) is a proxy for fresh traffic and combustion emissions and shows prominent peaks at m/z values 55 and 57 and a higher fractional organic signal at m/z 43 than m/z 44. For separation of cooking organic aerosol (COA) and distinguishing it from HOA in this study, we used the Robinson et al (2018) ratio of contributions at m/z 55:57 of 1.6 as a preliminary test for relative positioning of the HOA and COA profiles (COA factors with the ratio close to or greater than 1.6 and HOA profiles with the ratio substantially lower than 1.6). We also validated obtained PMF factors by correlation of factor time series with external tracers. We use two tracers for HOA-influence: CO and the fossil-fuel component of black carbon, BC_{FF}, estimated using the model of Sandradewi et al. (2008). For the time-series of BBOA factors, we use three tracers: (i) chloride (under the influence of agricultural and other open waste burning-related contributions (Li et al., 2014a, b; Kumar et al., 2015; Fourtziou et al., 2017), (ii) ΔC, defined as the difference between UVPM (370 nm) and BC detected by the aethalometer (Wang et al., 2011; Olson et al., 2015; Tian et al., 2019), and (iii) the biomass-burning component of black carbon, BC_{BB}, estimated using the model of Sandradewi et al. (2008). COA-related factors often exhibit weak correlations with external tracers (Huang et al., 2010, Sun et al., 2011, Liu et al., 2012, Sun et al., 2013, Hu et al., 2016, Stavroulas et al., 2019). Additionally, the EPA PMF tool provides detailed uncertainty analysis tools to validate how representative the chosen PMF solutions are for the respective time windows. Here, we use the uncertainty analysis to select PMF solutions and only finalize solutions that pass the EPA PMF tests of random error and rotational ambiguity, as described below in Sect. 2.5. The application of these detailed uncertainty analyses to select a PMF solutions for each time window, including the consideration of 3–8-factor solutions, is documented in Table S6, with supporting information in Tables S5, S7–S10.

2.5 Uncertainty estimation

In EPA PMF, quantitative error estimation (EE) of random error and rotational ambiguity was conducted using Bootstrapping (BS), Displacement (DISP), and Bootstrapping enhanced with Displacement (BS-DISP). This detailed uncertainty analysis ensures that the identified MS/TS are representative of the four-hour time windows by fitting 100s-10000s of PMF-like model runs to data subgroups within the four-hour time windows (Paatero et al., 2014). Detailed summary statistics from running these uncertainty analyses are presented as mappings onto the PMF solution for the entire time domain (Tables S8-S10). The

algorithms and computational workload of these techniques are described in detail elsewhere (Paatero et al., 2014). The application of these EE techniques leads to several orders of magnitude increase of computational time and memory requirements in conducting PMF runs (Paatero et al., 2014).

Bootstrapping or BS estimates "disproportionate effects of a small set of observations on the solution". In the process, BS accounts for random error and to a limited extent rotational ambiguity (Norris et al., 2014). EPA PMF automatically identifies BS datasets using the parameter "Block Size" that is based on the principle of stationarity and accounts for underlying serial correlations (Politis and White, 2004). The default calculation of the "Block size" in EPA PMF is based on incorrect calculations and updated calculations have been published (Patton et al., 2009) but not implemented in the EPA PMF tool. We used the corrected block size estimation procedure as shown in the Supplement (Sect. S2, Table S5). BS factors are then mapped to base factors using the parameter "Minimum Correlation R-Value", which is the minimum Pearson correlation coefficient used for BS factor assignment. We use the default value of 0.6 and conduct 100 BS runs for each PMF solution. Specification of too many factors in the base model may create artificial PMF factors (Ulbrich et al., 2009). BS factors with rotational ambiguity may also get mapped to other base factors. This scenario is called factor swapping and occurs for not-well-defined (NWD) solutions. These factors will likely have low BS mapping with their equivalent base run factors (Paatero et al., 2014). We only finalize PMF factor solutions with approximately 80% or more BS mapping for all PMF factors.

Displacement or DISP estimates rotational ambiguity in PMF solutions by identifying the range of allowable MS profile contributions in the PMF factors. Bootstrapping enhanced with Displacement or BS-DISP combines the bootstrap and displacement techniques to simultaneously estimate random error and rotational ambiguity in PMF solutions. In BS-DISP, BS resamples explore the solution space randomly and DISP explores the rotationally accessible space around each BS resample. The ranges in DISP are obtained corresponding to four limits on changes in the Q-value (dQ-max): 4, 8, 15, and 25. BS-DISP also reports ranges for contributions at different m/zs to MS profiles of PMF factors. These ranges correspond to four limits on changes in the Q-value (dQ-max): 0.5, 1, 2, and 4. The obtained PMF factors using both approaches are then mapped to base factors, and the number of cases of factor swaps are noted. Sometimes, DISP and BS-DISP runs are terminated when encountering large changes in the Q-value, which suggests the base case solution is not close to the global minimum. Generally, small changes in Q suggest PMF solutions are close to the global minimum. Additionally, small number of factor swaps suggest low rotational ambiguity and robustness of the PMF solution. We only finalize PMF solutions with very few swaps at the smallest dQ-max value. Some DISP and BS-DISP runs terminated due to computational limits or encountering high dQ-max. For these cases, we used the number of factor swaps at termination as an estimate of total factor swaps. Finally, even when solutions with factor swaps are encountered, only solutions with swaps among the lowest number of factors are considered interpretable (Norris et al., 2014). All other solutions are rejected.

3 Results and discussion

In this paper, we focus on the implementation of the time-of-day PMF technique on organic aerosol measured during monsoon midday and night periods and winter midday and night periods (Table 1). We report average concentrations of PMF factors in Table 2. For reference, data from seasonal PMF analysis are also presented. We find that time-of-day PMF analysis: (i) generates a larger diversity of primary factors than seasonal PMF, (ii) resolves mass spectra of cooking-related factors such as cooking organic aerosol (COA), mixed COA-HOA, and solid fuel combustion organic aerosol (SFC-OA) in Delhi, that are relatively unexplored (Tobler et al., 2020), and (iii) resolves different kinds of biomass burning organic aerosol (BBOA)-related factors (two BBOAs, one SFC-OA) based on MS and TS correlations (Sect. 3.3) (Table 2). Seasonal monsoon PMF analysis represents primary organic aerosol (POA) by a single hydrocarbon-like organic aerosol (HOA) whereas monsoon time-of-day PMF analysis represents midday POA as a mixed COA-HOA factor and nighttime POA as separate HOA and COA. In winter, seasonal PMF analysis separates POA into HOA and BBOA factors. In winter time-of-day PMF analysis, midday POA separates into an SFC-OA factor and a BBOA factor, and nighttime PMF analysis gives HOA and BBOA. All analyses generate two oxidized organic aerosol (OOA) factors. Time series of the different time-of-day PMF factors are shown in Figs. 1–2.

In Sect. 3.1, we discuss the mass spectral profiles (MS) and time series patterns (TS) of factors obtained in seasonal PMF analysis conducted for winter and monsoon. In Sect. 3.2, we discuss the mass spectral profiles and time series patterns of factors obtained in time-of-day PMF analysis conducted for winter and monsoon midday and nighttime periods. In Sect. 3.3, we contrast the mass spectra and time series patterns of primary and secondary PMF factors obtained from time-of-day and seasonal PMF analyses. The mass spectra of POA, a proxy for primary OA, and OOA, a proxy for secondary OA were calculated by adding the component factors corresponding to each type (e.g., POA = HOA + BBOA + COA) weighted by their respective time series contributions. This estimation allows a comparison between the results from the time-of-day and seasonal analyses. In Sect. 3.4, we compare the midday and nighttime POA and OOA MS profile results from the seasonal PMF and the time-of-day PMF approach. Our hypothesis is that the time-of-day PMF approach will show larger variability across the two time periods. In Sect. 3.5, we discuss period-specific Q (and $Q/Qexp$) values for the time-of-day PMF approach and the seasonal PMF approach. We also compare the $Q/Qexp$ TS patterns and $Q/Qexp$ by m/z to identify periods and m/zs with particularly significant changes in $Q/Qexp$.
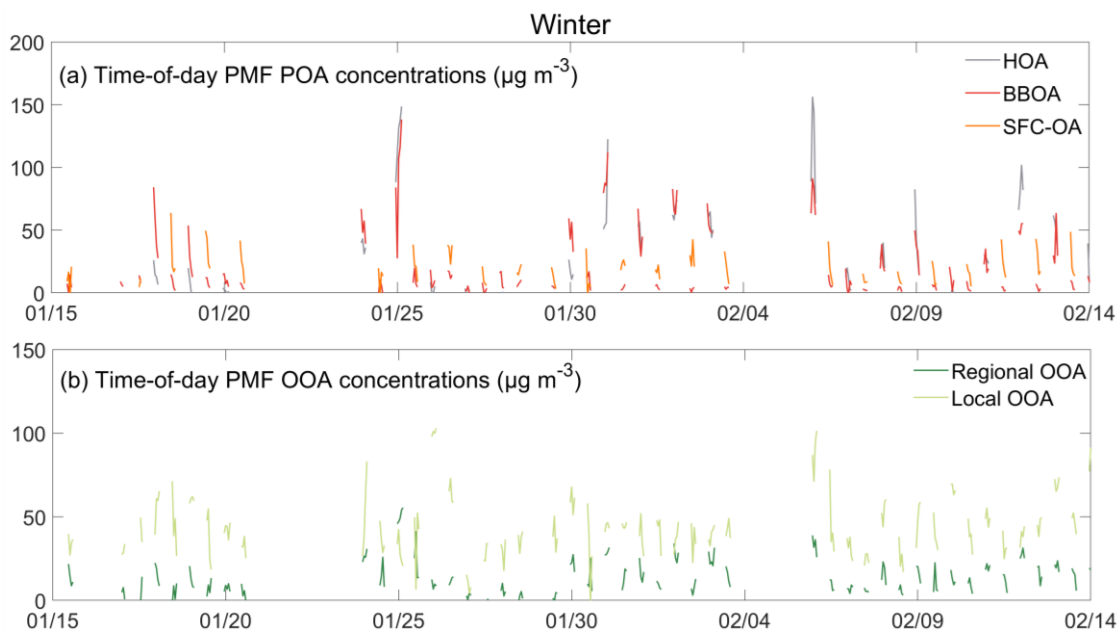
Figure 1. Hourly averaged seasonally representative concentration time series of time-of-day PMF (a) primary and (b) secondary factors for winter 2017 (in µg m⁻³). POA PMF factors show stronger variability than OOA PMF factors. (Chopped lines are due to the analysis conducted on two 4-hour periods each day.)
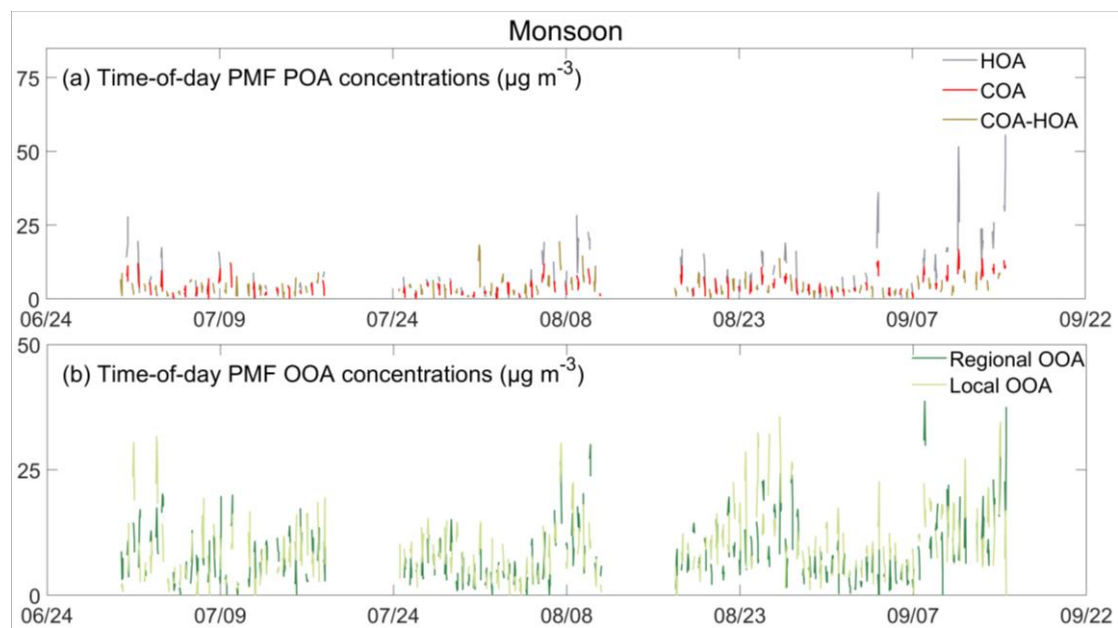

Figure 2. Hourly averaged seasonally representative concentration time series of time-of-day PMF (a) primary and (b) secondary factors for monsoon 2017 (in µg m⁻³). POA PMF factors show stronger variability than OOA PMF factors. (Chopped lines are due to analysis conducted on two 4-hour periods each day.)

Table 2 PMF factor concentrations in seasonal PMF and time-of-day PMF analysis (in µg m⁻³).

Season	Period	PMF Run Type	Factor Type	Factor Concentrations
M17	11-15	Seasonal	POA (HOA)	2.5 (2.5)
			OOA (Local OOA, Regional OOA)	18.7 (5.4, 13.3)
		Time resolved	POA (COA-HOA)	4.0 (4.0)
			OOA (Local OOA, Regional OOA)	17.4 (6.4, 11.0)
	23-03	Seasonal	POA (HOA)	8.8 (8.8)
			OOA (Local OOA, Regional OOA)	21.4 (10.7, 10.8)
		Time resolved	POA (HOA, COA)	12.1 (7.7, 4.4)
			OOA (Local OOA, Regional OOA)	17.8 (7.7, 10.0)
W17	11-15	Seasonal	POA (HOA, BBOA)	13.3 (3.5, 9.7)
			OOA (Local OOA, Regional OOA)	55.5 (13.0, 42.4)
		Time resolved	POA (SFC-OA, BBOA)	23.0 (18.1, 4.9)
			OOA (Local OOA, Regional OOA)	46.6 (37.6, 8.9)
	23-03	Seasonal	POA (HOA, BBOA)	86.3 (49.3, 37)
			OOA (Local OOA, Regional OOA)	56.5 (22.3, 34.2)
		Time resolved	POA (HOA, BBOA)	71.8 (35.5, 36.2)
			OOA (Local OOA, Regional OOA)	70.9 (18.7, 52.2)

3.1 Seasonal PMF runs

The analysis in this section focuses on the PMF factors from seasonal PMF analysis; since this work focuses on specific times of day, the results are presented only for the 1115 and the 2303 time windows. Due to differing meteorology, sources, and photochemistry, the factor speciation, their mass spectra, and their time series patterns are quite different in the two seasons. A comparison of POA and OOA in different seasons has been previously presented (Bhandari et al., 2020). In winter, seasonal PMF analysis results in two factors representing POA, namely HOA and BBOA, whereas only HOA is obtained in monsoon seasonal PMF analysis. In the two seasonal PMF runs, we also obtain two OOA factors: local (less oxidized) OOA and regional (more oxidized) OOA (Drosatou et al., 2019; Table 2).

The behaviour of the HOA factor MS is in line with the reference HOA factor MS, as suggested by the dominance of hydrocarbon signatures in the HOA spectrum belonging to the series C_nH_{2n-1+} and C_nH_{2n+1+} (Ng et al., 2011a; Bhandari et al., 2020; Pearson R~0.95; Figs. S4 and S5). In monsoon, the seasonal PMF HOA MS is also strongly correlated with the reference COA factor MS (Ng et al., 2011a; Pearson R~0.90; Fig. S5). However, the monsoon seasonal POA factor MS had a *m/z* 55 to

m/z 57 ratio of 1.2 (Fig. S5). Therefore, the seasonal monsoon POA factor is presented as an HOA factor. This HOA factor has stronger correlations with tracers CO (Spearman R: 0.73) and BC_{FF} (Spearman R: 0.91) than the OOA factors (Fig. S6). In winter, the fractional contributions of the BBOA factor MS at *m/z*s 60, 73, and 115 are in line with the reference BBOA factor MS (He et al., 2010; Crippa et al., 2014; Bertrand et al., 2017; Pearson R~0.90; Fig. S7). As expected, POA tracers, carbon monoxide (CO) and black carbon (BC), correlate more strongly with HOA and BBOA factor TS than with the OOA factor TS (Figs. S6 and S8). Additionally, BBOA correlates with chloride, particularly in the evening, suggestive of agricultural and other open waste burning-related contributions (Li et al., 2014a, b; Kumar et al., 2015; Fourtziou et al., 2017; Spearman R~0.70; Figs. S8 and S9). We also observe strong correlations of the local OOA factor with chloride (Spearman R~0.65; Fig. S8). These results are consistent with our previous seasonal organic-inorganic PMF analysis which suggested that chloride, associated with an oxidized BBOA factor (likely a combination of local OOA and BBOA) with weak BC_{BB} and ΔC correlations, might be linked to an industrial source (Bhandari et al., 2020). Indeed, chloride has weak correlations with BC_{BB} (Spearman R~0.45; Figs. S8 and S9).

OOA factors are principally associated with secondary organic aerosol (SOA; Zhang et al., 2011). Mass spectra of both local OOA and regional OOA correlate strongly with the reference OOA factor (Figs. S10–S11a–b; Pearson R≥0.95). However, local OOA correlates more strongly with the reference semi-volatile oxidized organic aerosol (SVOOA) factor (Zhang et al., 2011; Drosatou et al., 2019; Figs. S10 and S11; Pearson R~0.80). The time series of the regional OOA factor correlates stronger with sulfate, whereas local OOA correlates stronger with chloride and black (BC) and brown carbon (UVPM) (Figs. S6 and S8). Overall, regional OOA shows less diurnal variability than local OOA, in line with a regional origin (Figs. S12 and S13). Detailed 15 min time series patterns of seasonal PMF factors for the midday (1115) and nighttime (2303) periods in the two seasons are discussed in the Supplement (Sect. S3).

3.2 Time-of-day PMF runs

The analysis in this section focuses on the PMF factors from time-of-day analysis for the 1115 and the 2303 time windows. Here, we show that time-of-day PMF analysis resolves mass spectra of cooking- and biomass burning-related factors (one COA, one mixed COA-HOA, one SFC-OA, two BBOAs) based on MS and TS correlations. Only nighttime periods separate clean HOA factors.

3.2.1 Primary factor MS and TS

<u>Winter 2017 Primary factor MS</u>

At winter midday, PMF analysis results in two factors representing POA, SFC-OA and BBOA, whereas at nighttime, HOA and BBOA are obtained (Table 2). The behavior of the winter time-of-day PMF HOA factor MS is in line with the reference HOA factor MS (Ng et al., 2011a; Pearson R>0.95; Fig. S17a). The MS of the winter BBOA factors obtained are correlated with the reference profile but differ in contributions at key *m/z* values such as *m/z*s 29, 43, and 44 (Pearson R≥~0.8; Fig. S16b, S17b). Both MS profiles show much larger *m/z* 29 contributions than the reference profile, suggesting a strong influence of

wood burning (Bahreini et al., 2005; Schneider et al., 2006). The winter midday BBOA is more oxidized (MS shows higher ratio of contributions at m/z 44 to m/z 43) and shows a low m/z 60 contribution. It also has a high contribution at m/z 15 (Fig. S16b). Similar BBOA MS profiles with high m/z 15 have been observed previously as well (Crippa et al., 2013). In contrast, the winter nighttime BBOA is less oxidized and BBOA MS shows an m/z 60 contribution closer to the higher end of the reference profile (Fig. S17b). At midday in winter, we also obtain a mixed POA factor (Fig. S16a). We call it solid fuel combustion organic aerosol (SFC-OA) as the factor MS correlates with multiple reference MS profiles such as BBOA, HOA, and COA (Pearson R>0.8). This behaviour is similar to a seasonal PMF SFC-OA factor identified recently in ToF-ACSM analysis for NR-PM$_{2.5}$ in Delhi. In that study, that factor was expected to be associated with heating- and cooking-related domestic fuel combustion and open-fire activities (Tobler et al., 2020; correlation at all m/zs but m/z 44, Pearson R>0.95; Fig. S18).

Monsoon 2017 Primary Factor MS

At midday in monsoon, we see only one POA factor, COA-HOA (Fig. S19). COA-HOA MS shows similarities with both the reference COA and HOA MS (ref. COA: Pearson R~0.90, ref. HOA: Pearson R~0.80; Fig. S19). The inability to separate HOA and COA factors for mass spectral data obtained in a major city in the Indo-Gangetic Plains has been observed previously as well (Thamban et al., 2017; Bhandari et al., 2020). However, a key difference of this factor compared to the reference HOA and COA profiles are the large contributions at m/z 44 in monsoon midday COA-HOA. These high contributions are likely a result of the highly oxidizing environment in the afternoon. Afternoon overlaps with periods of high shortwave radiative flux (SWR) and therefore high reactivity of the atmosphere (Fig. S1). At monsoon nighttime, HOA and COA separate out (Fig. S20a–b). The behavior of the monsoon nighttime time-of-day PMF HOA factor MS is in line with the reference HOA factor MS (Ng et al., 2011a; Pearson R>0.95; Fig. S20a). The monsoon nighttime COA factor MS is very similar to the reference COA factor MS (Pearson R~0.90; Robinson et al., 2018, ratio of contributions at m/z 55 to m/z 57~1.66; Fig. S20b). A key feature of this COA factor is the high m/z 41, a characteristic feature of COA from heated cooking oils, especially in Asian cooking (Allan et al., 2010; Liu et al., 2018; Zhang et al., 2020; Zheng et al., 2020).

Primary Factor TS

CO and BC serve as tracers for HOA, BBOA, and SFC-OA (Figs. S21–S24). The winter midday SFC-OA profile correlates strongly with chloride (Spearman R: 0.71), nitrate (Spearman R: 0.75), BCFF (Spearman R: 0.79), and ΔC (Spearman R: 0.60), pointing to the mixing of HOA, BBOA, and possibly COA in the factor (Fig. S21). At winter nighttime, we separate an HOA MS profile that correlates strongly with BCFF (Spearman R: 0.84) and CO (Spearman R: 0.83) (Fig. S22). We obtain one BBOA factor each at winter midday and winter nighttime. Among the two BBOA obtained, winter midday BBOA correlates strongly with chloride (Spearman R: 0.66) and CO (Spearman R: 0.67), suggesting an industrial source (Fig. S21, Sect. 3.1). At nighttime, however, winter BBOA correlates strongest with the wood burning component of BC (BC$_{BB}$, Spearman R: 0.92) and weakly with chloride (Spearman R: 0.40), suggesting at least two different origins of BBOA (Fig. S22). This is consistent with our previous work, where we have separated BBOA-like factors with different correlations with chloride and BC$_{BB}$ in

different seasons (Bhandari et al., 2020; Patel et al., 2021a). In monsoon midday, we observe only one primary factor, a COA-HOA factor, with strong correlations with chloride (Spearman R: 0.75), suggesting the influence of landfill emissions, trash burning, and solid-fuel sources (Fig. S23; Dall'Osto et al., 2015, Lin et al., 2017). Otherwise, COA-HOA has weak correlations with external tracers. Similar behaviour of COA-dominated factors has been seen previously as well (Huang et al., 2010, Sun et al., 2011, Liu et al., 2012, Sun et al., 2013, Hu et al., 2016, Stavroulas et al., 2019). In the monsoon nighttime PMF run (M-23-03), we observe stronger correlations of the HOA factor with CO (Spearman R: 0.79) and BC_{FF} (Spearman R: 0.86) compared to correlations of these tracers with the COA factor (CO: Spearman R: 0.70, BCFF: Spearman R: 0.71; Fig. S24).

3.2.2 Secondary factor MS and TS

Time-of-day PMF and seasonal PMF generate two OOA factors, local OOA and regional OOA, in each run (Figs. S25 and S26). Typically, regional OOA is more oxidized (shows weaker correlations with reference SVOOA MS) and has less diurnal variation, in line with its expected average lower volatility and contributions from long-range transport (Drosatou et al., 2019). The time-of-day PMF OOA factors show MS and TS behaviour similar to the seasonal PMF OOA factors, as shown in Sect. 3.3. Mass spectra of both local OOA and regional OOA correlate strongly with the reference OOA factor (Pearson R>~0.80; Figs. S25 and S26). Also, we consistently observe that the more oxidized regional OOA factors have flatter diurnal time series patterns (smaller range) than the less oxidized local OOA factors (larger range) (Figs. S27–S30; Table S11). However, we see an overlap of the 95% confidence intervals of the normalized levels of the local and regional OOA factors (Figs. S27–S30) and an overlap of external tracers suggesting mixing of the two OOA components (see Sect. S4). This is not surprising considering the similarity of MS of the two OOA factors and a continuum of the level of oxidation in the atmosphere (Drosatou et al., 2019).Since we observe factor mixing of the two secondary components, detailed analysis of the factor MS and TS (correlations with external tracers, features of the mass spectra) are only presented in the Supplement (see Sect. S4).

3.2.3 Time series patterns of time-of-day PMF factors

Time series patterns exhibit contrasting behaviour in winter and monsoon time-of-day PMF analysis, similar to the seasonal factor contrast (Sect. S3; Figs. 3–4a–b). Midday, concentrations of all primary factors exhibit a monotonically decreasing pattern likely due to increasing ventilation (Figs. 3a, 4a, S1). In the midday period, winter peak SFC-OA and BBOA concentrations are both ~3 times the period minimum (Fig. 3a). At winter night, peak concentrations of HOA and BBOA are ~2.5 times and ~3 times the period minimum (Fig. 3b). In contrast, monsoon primary factors exhibit lower variability midday (peak COA-HOA concentrations~2 times the period minimum) and nighttime (peak HOA~2.5 times the period minimum; peak COA~2 times the period minimum).

Additionally, the nighttime factors in both seasons show larger differences between the mean and the median than the corresponding midday factors in the same seasons, which suggests episodic nature of factors. The presence of episodes in these primary factors could be a consequence of the temperature-related inversions at nighttime, which lead to aerosol accumulation (Bhandari et al., 2020). These episodes could also be a result of episodic sources contributing to these factors.

465   Generally, HOA shows the largest mean-median differences, and episodic contributions could be from heavy duty vehicles, brick kilns, and construction and road paving activities (Guttikunda et al., 2013; Dallmann et al., 2014; Mishra et al., 2019; Khare et al., 2020; Misra et al., 2020). For BBOA, these sources could be associated with burning events, as hypothesized previously (Bhandari et al., 2020). Episodic events could also be due to precipitation (Fig. S1). OOA factors experience mixing, so their time series patterns are not discussed.

470
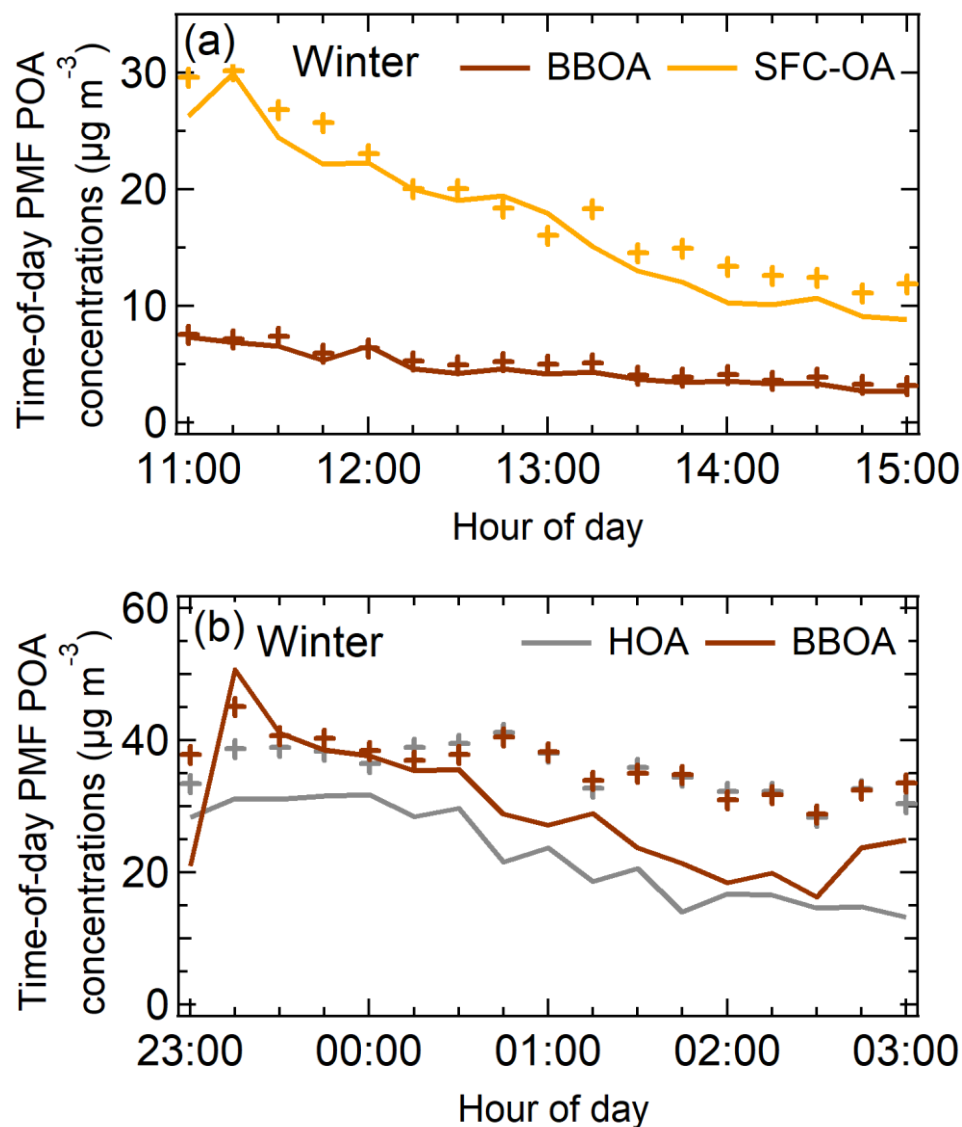
Figure 3 shows 15 min averaged seasonally representative mean (+) and median concentrations (lines) of time-of-day PMF primary factors for the periods: (a) W-11-15 and (b) W-23-03 (in μg m^{-3}). Nighttime factors show evidence of episodes.

3.3 Comparisons of POA and OOA MS and TS obtained using time-of-day PMF and seasonal PMF

475 Results from the previous sections show that time-of-day PMF analysis generates a larger diversity of factors compared to seasonal PMF analysis. In this section, we summarize and compare the primary and secondary MS and TS contributions of factors using PMF results from two approaches—seasonal PMF and time-of-day PMF analysis. We show that (i) seasonal PMF analysis significantly underestimates primary concentrations at midday compared to time-of-day analysis (Tables 2 and 3; Figs. 5–6a–b), (ii) midday shows cleaner signatures in POA factor MS in time-of-day PMF analysis compared to the seasonal

480 PMF analysis (Figs. 7–8a–b), and (iii) nighttime OOA MS and TS show larger differences between the two techniques than nighttime POA MS and TS, whereas midday shows larger differences in POA than OOA (Table 3, Figs. 7–8a–b, S31–S36). We also observe larger differences of the POA mass spectra from the two techniques midday than at night (Figs. 7–8a–b). Detailed MS and TS comparisons of time-of-day PMF POA and OOA with the seasonal PMF results are discussed below.
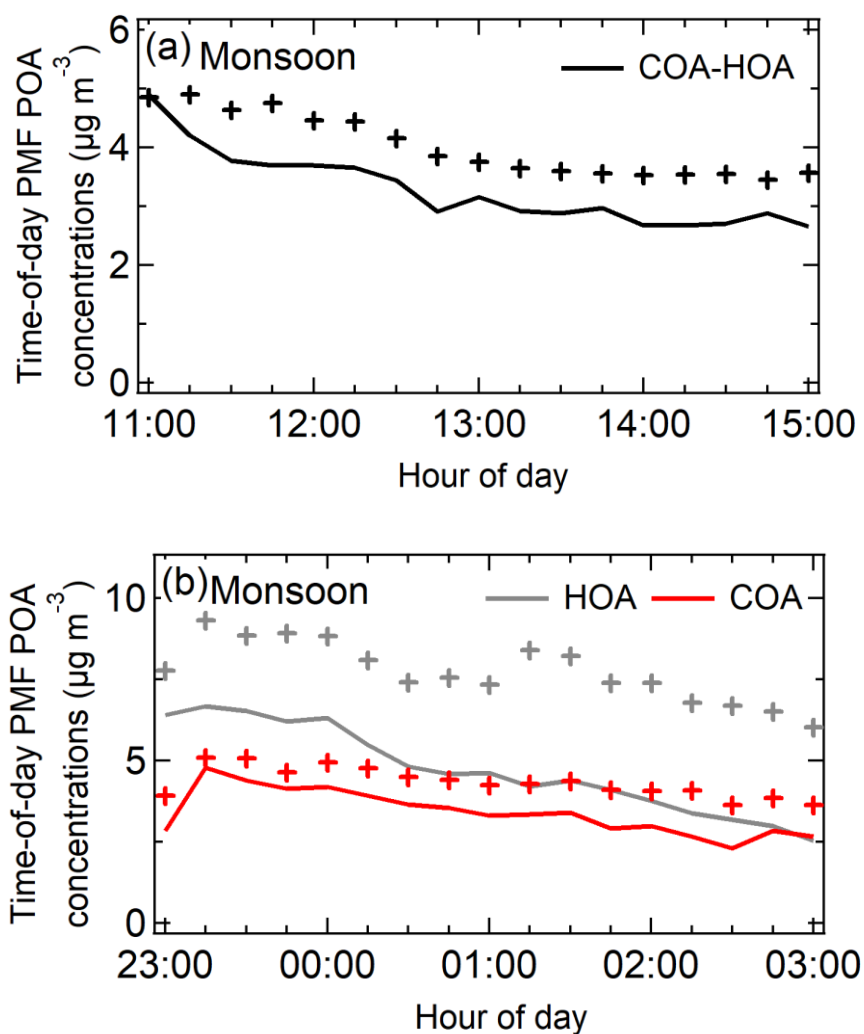
485

Figure 4 shows 15 min averaged seasonally representative mean (+) and median concentrations (lines) of time-of-day PMF primary factors for the periods: (a) M-11-15 and (b) M-23-03 (in µg m^{-3}). Nighttime HOA shows stronger episodes than COA.

490

Table 3 Time series correlations of time-of-day POA and OOA TS with seasonal POA and OOA TS

Period	Factor Type	Pearson R	Slope/intercept with the corresponding seasonal POA/OOA TS
W-11-15	POA	0.96	1.38/4.7
	OOA	0.96	0.77/3.9
W-23-03	POA	1.00	0.94/-9.2
	OOA	0.98	1.19/3.4
M-11-15	POA	0.86	1.04/1.4
	OOA	0.99	0.99/-1.2
M-23-03	POA	0.99	1.12/2.3
	OOA	0.99	0.86/-0.6

Here, we show that the time-of-day PMF approach shows strong similarities in time series patterns of primary factors compared to seasonal PMF analysis. However, the two approaches show substantial time-of-day dependent differences in detected mass
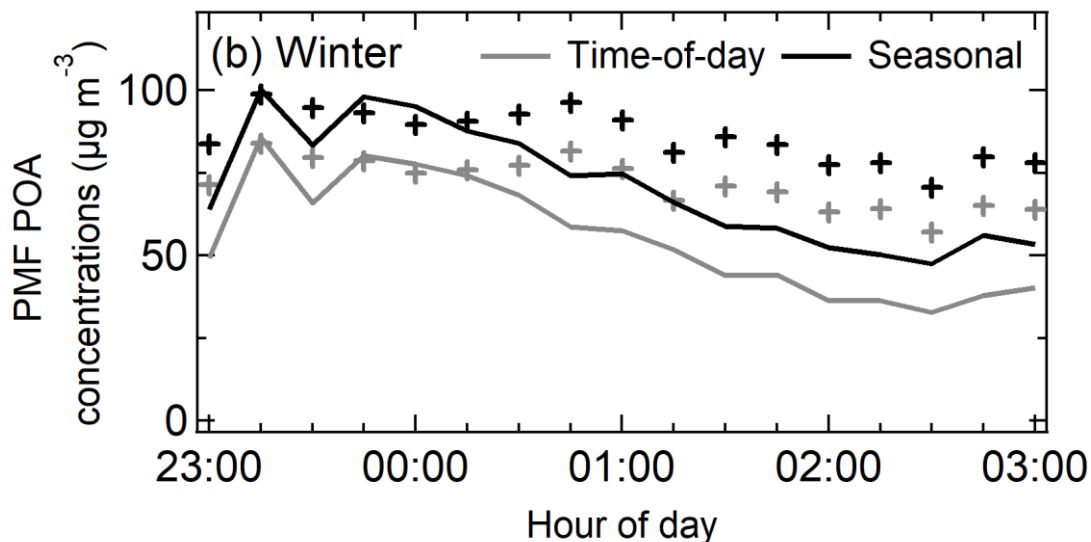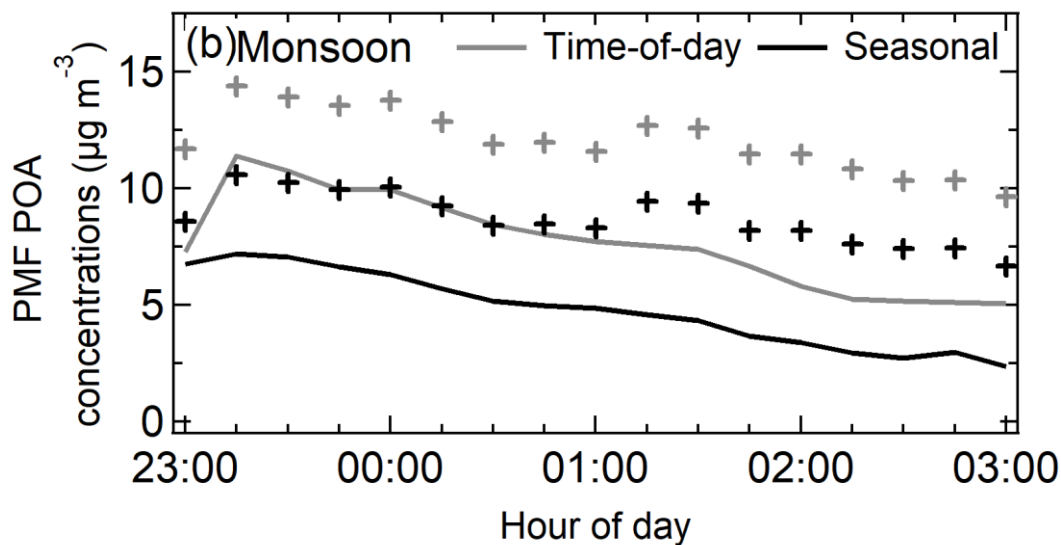
495   spectra.

19
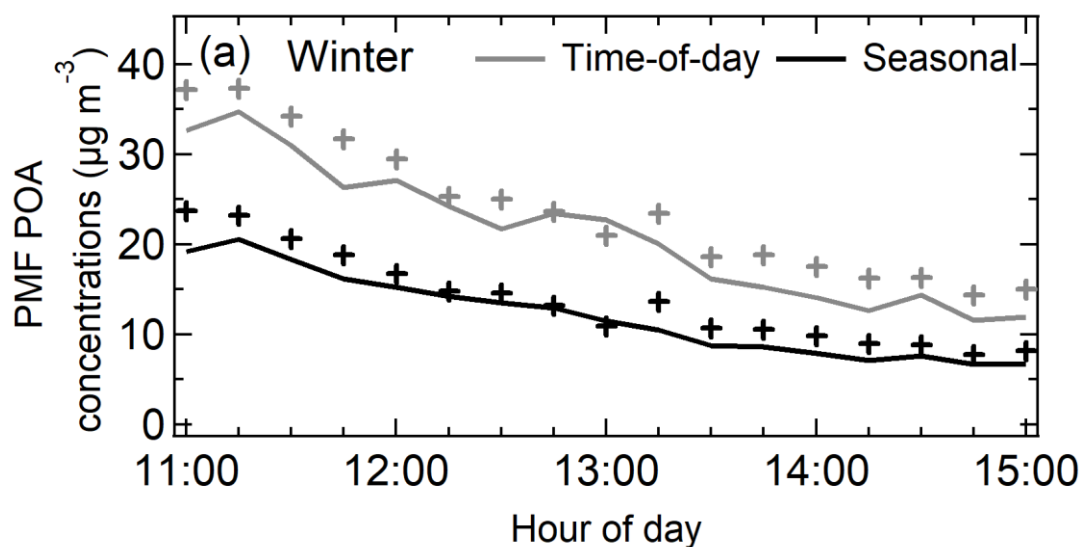
Figure 5 shows 15 min averaged seasonally representative diurnal mean (+) and median (lines) concentration time series of POA for the periods: (a) W-11-15 and (b) W-23-03 (in µg m⁻³). Nighttime factors show evidence of episodes.

500 **3.3.1 Comparison of POA time series**

The behaviour of POA is consistent with the individual component primary factors. POA is monotonically decreasing in all periods, concentrations are more variable during the day, and nighttime concentrations are several times those of midday concentrations (Figs. 5–6a–b). We observe striking similarities of the 15 min averaged time series patterns of POA between the two techniques across all periods (Table 3, Pearson R>0.85). The strong linear correlations suggest that time-of-day PMF

505 analysis results in shifted (but correlated) TS patterns.

3.3.2 Comparison of POA mass spectra

The time-of-day PMF approach generates POA mass spectra both similar and different from the seasonal PMF approach, depending on the time-of-day (Figs. 7–8a–b). Two features stand out in these comparisons: the midday POA MS are dissimilar at key *m/z*s whereas the nighttime POA MS are nearly identical.
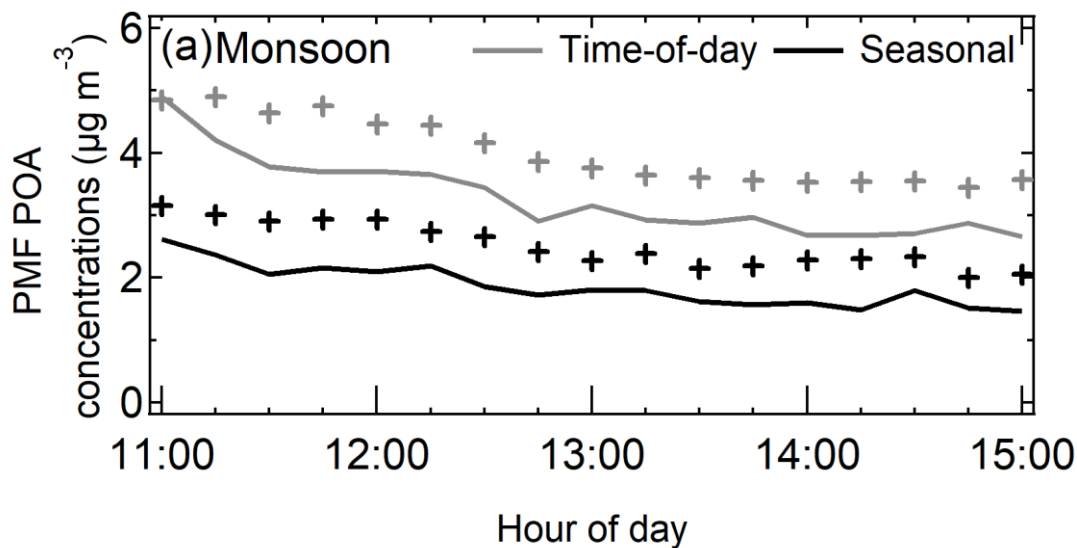
20

Figure 6 shows 15 min averaged seasonally representative diurnal mean (+) and median (lines) concentration time series of POA for the periods: (a) M-11-15 and (b) M-23-03 (in µg m⁻³). nighttime factors show stronger evidence of episodes.

Figures 7–8a–b show the MS pattern of time-of-day PMF POA and seasonal PMF POA at winter midday and nighttime (Fig. 7a–b) and monsoon midday and nighttime (Fig. 8a–b). In time-of-day PMF POA presented here, we observe a lower ratio of contributions at m/z 43 to m/z 44 than seasonal PMF POA. This lower ratio is indicative of the more oxidized nature of the POA factor compared to the seasonal POA (Ng et al., 2010). At midday, we observe higher contributions in time-of-day PMF POA at m/z 44; in line with the high photochemical processing (SWR flux, Fig. S1). We also observe a higher ratio of contributions at m/z 55 to m/z 57, and lower contributions at m/z 57 (Figs. 7a and 8a). These observations are in line with a

21

strong cooking influence (and lower traffic influence) at midday (Ng et al., 2011a; Robinson et al., 2018). At winter midday, we also observe lower contributions at m/zs 29, 60, and 73 in time-of-day PMF than seasonal PMF (Bahreini et al., 2005; Schneider et al., 2006). This observation is likely a consequence of the removal of the influence of wood burning for nighttime space heating on the time-of-day PMF POA MS for midday. At monsoon midday, we observe a higher contribution at m/z 41 than m/z 43 in time-of-day PMF POA, which is indicative of the influence of cooking (Allan et al., 2010; He et al., 2010). This POA also shows higher contribution at m/z 29, suggesting a higher influence of wood burning, likely associated with midday cooking. At nighttime, the differences between the time-of-day and seasonal profiles are much smaller. Overall, time-of-day PMF analysis seems to be capturing very specific features of primary aerosol behaviour better than seasonal PMF analysis.
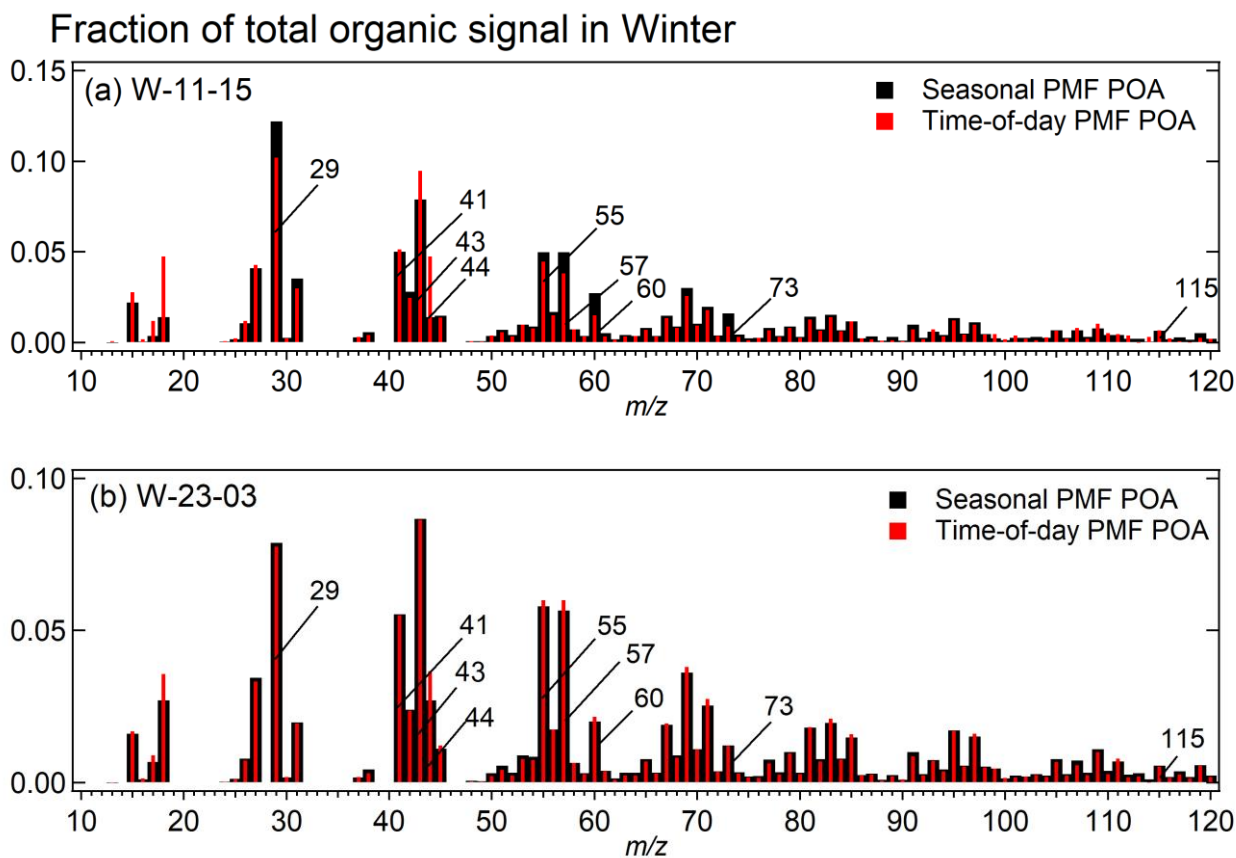
Figure 7 shows the mass spectra of time-of-day PMF POA and seasonal PMF POA for the periods (a) midday and (b) nighttime in winter 2017. Midday MS shows larger differences compared to nighttime MS.
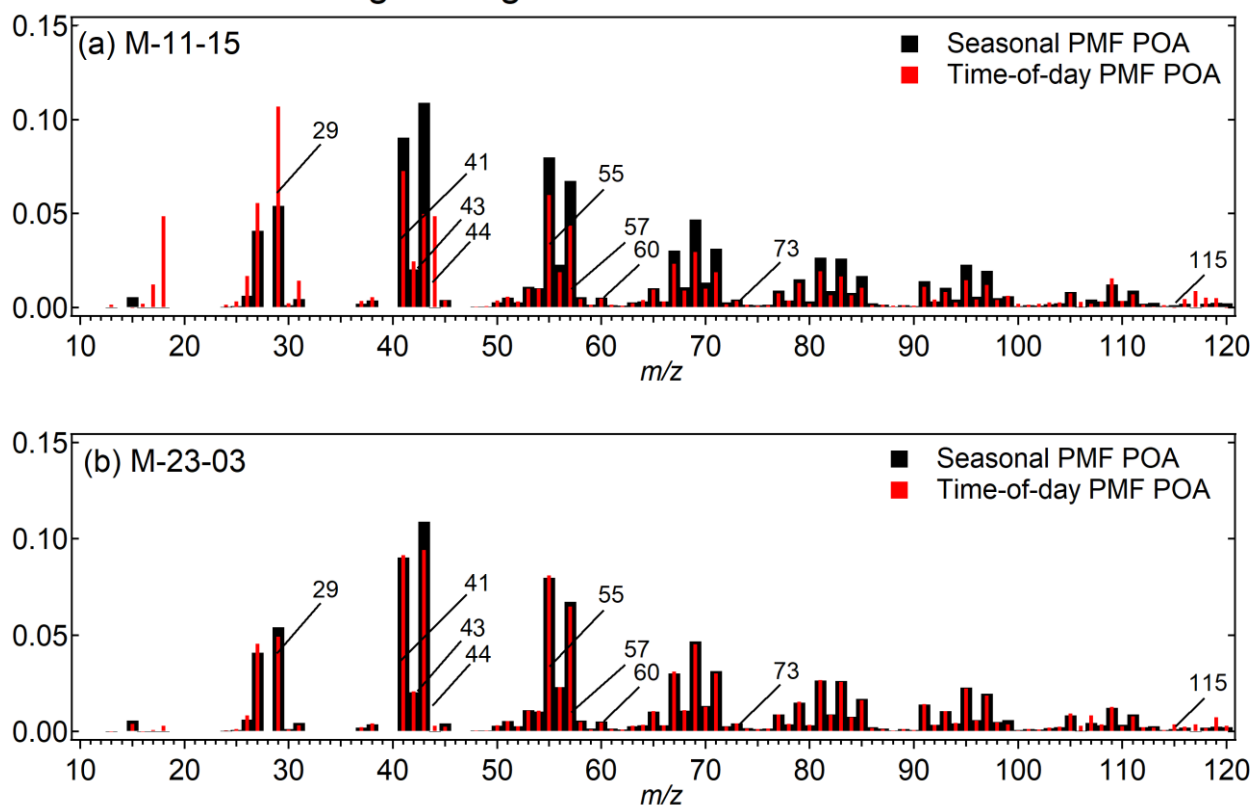
Figure 8 shows the mass spectra of time-of-day PMF POA and seasonal PMF POA for the periods (a) midday and (b) nighttime in monsoon 2017. Midday MS shows larger differences compared to nighttime MS.

540   3.4 Differences in midday and nighttime POA and OOA MS within time-of-day PMF versus seasonal PMF

We can also compare midday and nighttime POA MS from the time-of-day PMF analysis and the seasonal PMF analysis (Figs. S35–S36a–b). For both seasons, the two comparisons (seasonal PMF and time-of-day PMF) of midday and nighttime POA MS indicates more primary nature at nighttime than midday, based on the higher contributions at the m/zs corresponding to the alkyl hydrocarbons associated with primary combustion (Zhang et al., 2011). However, this contrast is sharper in time-of-

545   day PMF analysis, in line with the ability of the approach to capture variable MS (Figs. S35b and S36b; Fig. S39, Winter midday and nighttime POA MS: Time-of-day PMF Spearman R: 0.93, Seasonal PMF Spearman R: 0.97; Fig. S40, Monsoon midday and nighttime POA MS: Time-of-day PMF Spearman R: 0.81, Seasonal PMF Spearman R: 1.0). The seasonal PMF midday–nighttime comparison also fails to capture the influence of cooking midday based on the low and similar ratio of contributions at m/z 55 to m/z 57 at nighttime, esp. in monsoon (~1, Figs. S35a and S36a). This contrast between midday and

550   nighttime POA MS is higher in time-of-day PMF in winter (midday ratio: 1.2, nighttime ratio: 1.0, Fig. S31b) and in monsoon time-of-day PMF analysis (midday ratio: 1.4, nighttime ratio: 1.2, Fig. S36b). While seasonal PMF analysis for monsoon

suggests no change in MS between midday and nighttime, time-of-day PMF analysis suggests large shifts in contributions at key m/zs such as 41, 43, 44, 55, and 57, in line with the changing importance of cooking from midday to night. These differences demonstrate the ability of time-of-day PMF to capture variable MS corresponding to the source influence of those time-of-day periods (Sect. 3.3.2).

We can also compare OOA MS and TS as well as conduct midday and nighttime comparisons for time-of-day PMF and seasonal PMF analysis (Sect. S4; Figs. S37–S38a–b). Time-of-day PMF OOA MS and TS are similar to seasonal PMF OOA (Table 3, TS: Pearson R>0.95; Figs. S25-S26, MS: Pearson R≥0.95).However, the mass spectra of the time-of-day PMF OOA have major differences at m/z 44 relative to the seasonal PMF OOA (Figs. S33–S34a–b). Comparisons of midday and nighttime time-of-day PMF OOA MS show interesting patterns not apparent in seasonal PMF analysis (Figs. S37–S38a–b). For example, time-of-day PMF analysis for monsoon 2017 suggests less oxidized OOA at midday than nighttime, likely caused by the presence of semi-volatile compounds (Fig. S38b). Similar behaviour has been observed elsewhere as well, and was attributed to biogenic emissions (Canonaco et al., 2015).

Figure S39 shows all PMF factors obtained in this paper on the triangle plot (Ng et al., 2010). We observe that factors obtained in the time-of-day PMF analysis occupy a larger spread compared to those obtained in seasonal PMF analysis. For example, in time-of-day PMF POA factors, we observe a spread of about 5% in contributions at m/z 43. In contrast, the spread of seasonal PMF POA factors is less than 3%. Overall, because time-of-day PMF conducts PMF analyses for each period independent of the influence of the variability in the other periods, it generates more representative MS for each time-of-day period (Sect. 3.3).

3.5 Quantification of quality of fit using Q and $Q/Qexp$ patterns

As discussed in the methods section, PMF iterates to identify minima in the Q value, a residual-based metric often used as a measure of the quality of fit of the PMF solution (Sect. 2.2). Here, we compare the time-of-day PMF and the seasonal PMF approaches based on their Q and $Q/Qexp$ patterns. We show that Q and $Q/Qexp$ are lower in time-of-day PMF analysis than seasonal PMF analysis. By allowing the MS to change substantially relative to the seasonal profile at specific times of day, the time-of-day PMF lowers the residuals and therefore the Q values. These improvements in Q are (i) larger in winter compared to monsoon, (ii) larger at midday than nighttime, and (ii) are non-monotonic within the time-of-day periods.

3.5.1 Comparison of average Q and $Q/Qexp$ in different time-of-day periods

In Table 4, we compare the average Q and $Q/Qexp$ values obtained in the time-of-day PMF analysis and the seasonal PMF results. Our results indicate that time-of-day PMF approach significantly improves Q by 6–55% and $Q/Qexp$ by 5–30% of the original Q and $Q/Qexp$ values, respectively. A part of the improvement in Q going from seasonal PMF to time-of-day PMF is also due to the lower number of points and therefore, lower degree of freedom, as well as larger number of weak m/zs (Paatero et al., 1994; Paatero et al., 1997; Ulbrich et al., 2009; Table S3). However, decreases occurring in $Q/Qexp$ are less affected by the different number of weak m/zs, and validate the improvement (Table 4). Winter midday observes larger seasonal Q and

24

Q/Qexp values than monsoon midday despite lower number of time series points at winter midday. This result is likely an effect of the larger diversity of sources expected in winter, and a limitation of seasonal PMF to capture sources through static MS profiles (Paatero et al., 2002). Drops in monsoon and winter midday *Q/Qexp* (going from seasonal PMF to time-of-day PMF) are likely an outcome of the factor switching from only HOA to cooking-related factors (COA-HOA and SFC-OA, respectively). Further, even though seasonal *Q/Qexp* at winter nighttime is higher than monsoon nighttime, time-of-day *Q/Qexp* is similar. Improvements at nighttime comes primarily from a change in the OOA MS, as shown in Sect. 3.3. Thus, time-of-day PMF results in large improvements in fit relative to the seasonal PMF analysis.

Table 4 Comparison of average *Q* and *Q/Qexp* in time-of-day PMF and seasonal PMF

Period	Seasonal PMF *Q*[a]	Time-of-day PMF *Q*	Seasonal PMF *Q/Qexp*[a]	Time-of-day PMF *Q/Qexp*	% Change *Q*	% Change *Q/Qexp*
M-11-15	288030	241858	1.84	1.74	-16%	-5%
M-23-03	333134	313170	2.16	1.93	-6%	-11%
W-11-15	369452	164975	4.36	3.05	-55%	-30%
W-23-03	197984	161468	2.37	1.95	-18%	-18%

[a]The seasonal PMF *Q* (and *Q/Qexp*) values in these columns correspond to the *Q* (and *Q/Qexp*) values associated with the solution space of the respective time-resolved windows only. For details, refer to Sect. 2.2 Eqs. 16–17.

3.5.2 Comparison of time series patterns of *Q/Qexp* in different time-of-day periods

We can further explore the time periods and *m/z*s that show improvement in fits in the time-of-day PMF approach. In Fig. 9a–b, we plot the percent change of 15 min averaged *Q/Qexp* values from the seasonal PMF approach to the time-of-day PMF approach in the midday and nighttime periods. Monsoon results show limited variability, with the standard deviation (SD) of the percent change less than 5% from the mean (excluding the edges). On the other hand, in winter, the SD of the percent change are ≥15% from the mean, and time-of-day PMF approach particularly improves the solution in the middle of the midday window (11:30–14:00 LT) and the first half of the nighttime window (23:30–00:45 LT). These selective improvements suggest that time-of-day PMF likely accounts for period-specific sources better than the seasonal PMF approach.

3.5.3 Comparison of *Q/Qexp* by *m/z* in different time-of-day periods

Instead of classifying improvements in *Q/Qexp* by time, we can classify the improvements by *m/z*s. In Fig. 10a–b, we plot the percent change of *Q/Qexp* at different *m/z*s between the seasonal PMF approach and the time-of-day PMF approach. Our results show that the percent changes are either negative or small positive at important *m/z* tracers in all periods. In addition, the changes are largely negative at *m/z*s higher than *m/z* 80, suggesting that time-of-day PMF approach particularly improves the fits at *m/z*s higher than *m/z* 80. In particular, winter midday is accompanied by decreases at important *m/z*s such as 29, 41, 43, 44, 55, 57, and 60, as well as *m/z*s higher than *m/z* 80.

We also observe that the fit quality reduced at some m/zs; however, most of these m/zs are not tracers of specific PMF factor types (Zhang et al., 2011). Future work could investigate the deployment of the binPMF approach, selectively fitting important m/zs only to identify PMF factors (Zhang et al., 2019). Overall, the time-of-day PMF approach improves PMF fit dissimilarly at different m/zs compared to the seasonal PMF approach.
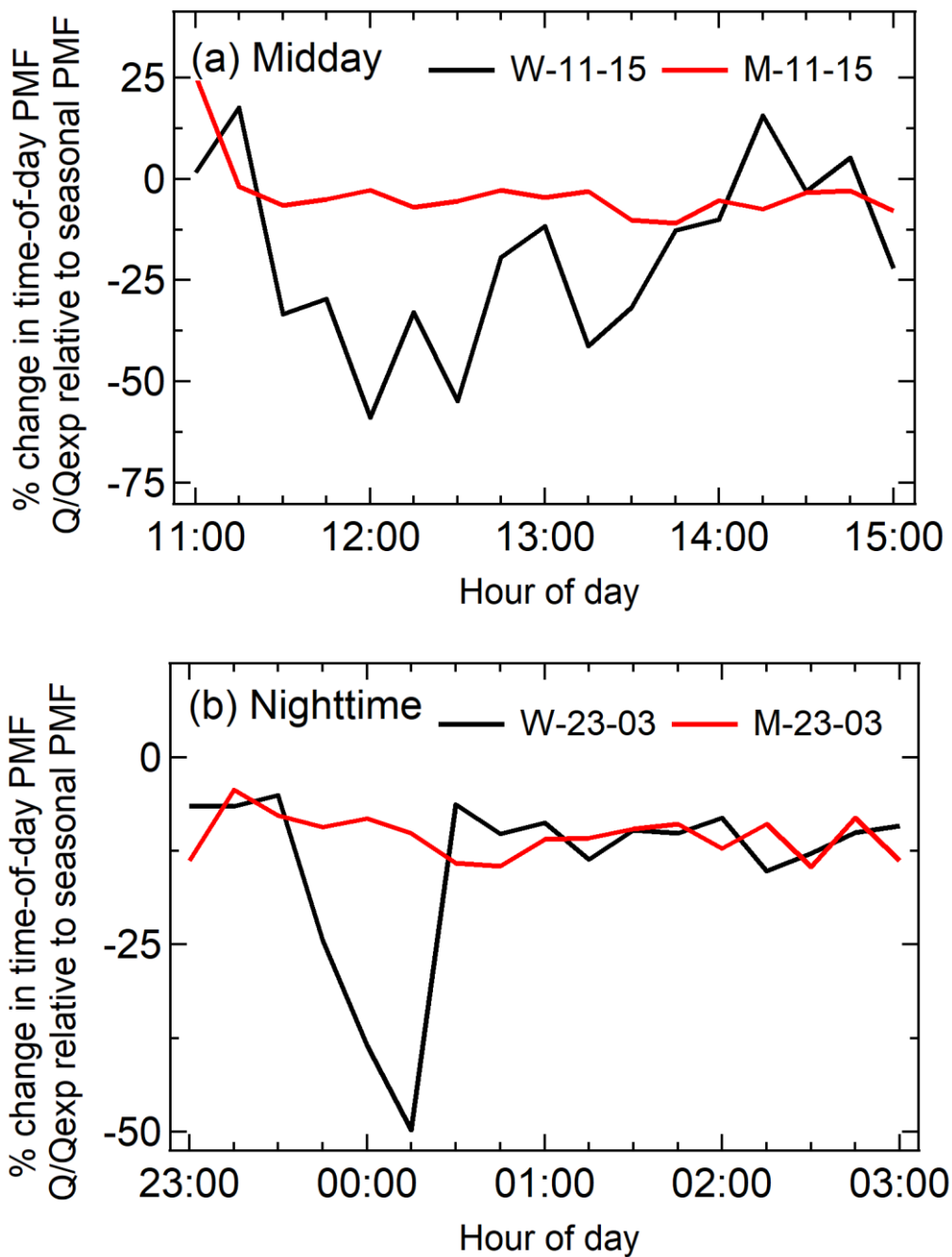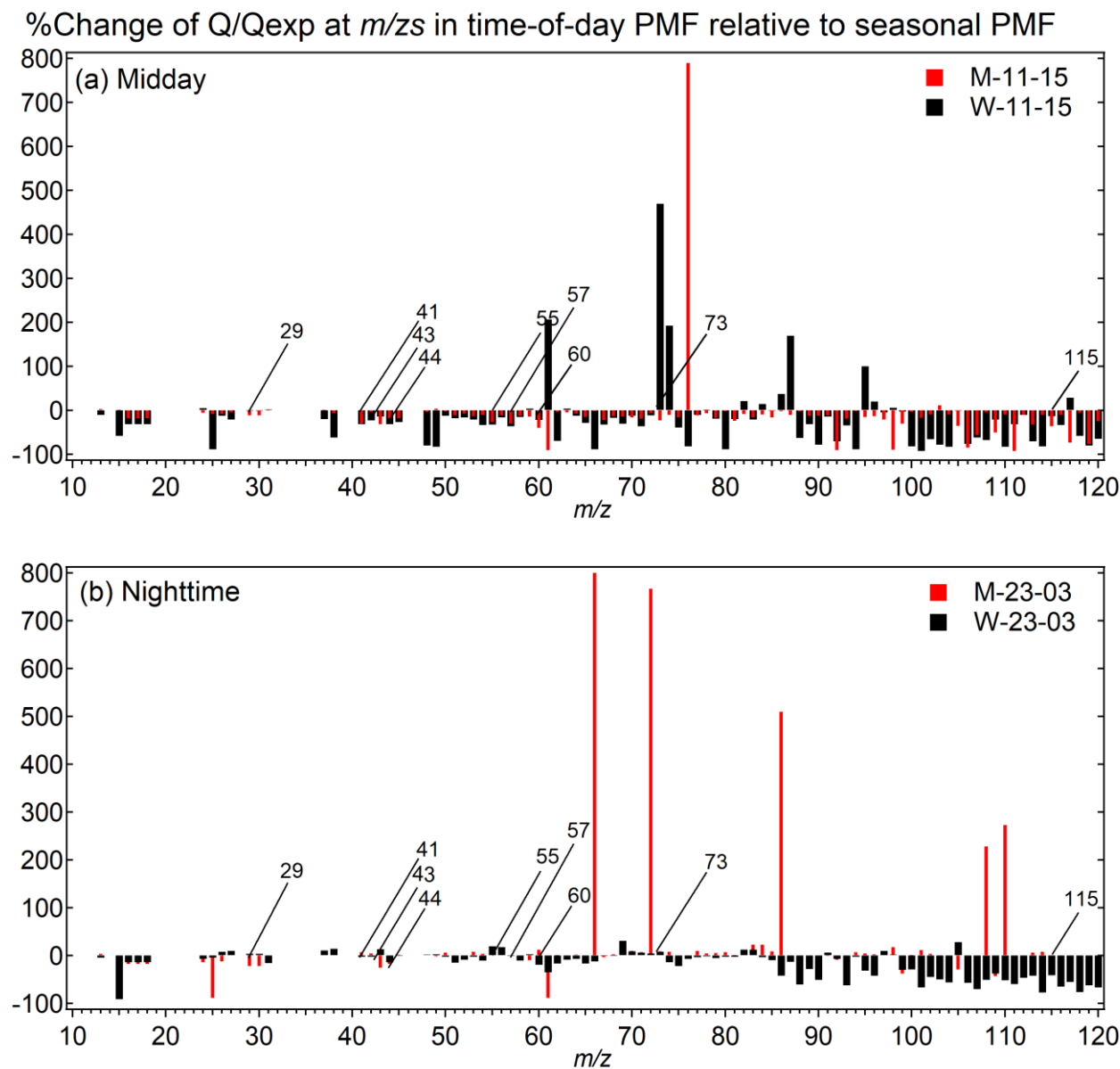
Figure 9 Percent change of 15 min averaged seasonally representative *Q/Qexp* values between the seasonal PMF approach and the time-of-day PMF approach in (a) midday and (b) nighttime periods. Time-of-day PMF selectively improves *Q/Qexp* in specific periods compared to the seasonal PMF approach.

Figure 10 shows the percent change of *Q/Qexp* at different *m/z*s between the seasonal PMF approach and the time-of-day PMF approach in (a) midday and (b) nighttime periods. Key *m/z*s show a lower *Q/Qexp* in the time-of-day PMF approach compared to the seasonal PMF approach.

Section 4 Conclusions

This study introduces a new approach to conducting source apportionment analysis—conducting positive matrix factorization on long-term datasets with each day separated into six 4 hour periods with limited variability in emissions and meteorology. The statistical viability of this new source apportionment approach is demonstrated, and the approach is called time-of-day PMF. We apply the time-of-day PMF approach on two seasons of highly time-resolved speciated non-refractory submicron aerosol (NR-PM$_1$) organics (Org). This dataset was collected as a part of the Delhi Aerosol Supersite (DAS) study. This study improves upon the seasonal source apportionment previously employed in Delhi. We use the EPA PMF tool to apply constraints, extract a larger number of factors, and quantify errors in PMF solutions.

Time-of-day PMF analysis resolves a greater diversity of factors compared to the traditional seasonal PMF approach. In winter, time-of-day PMF separates a mixed SFC-OA factor and a BBOA factor at midday but separates clean HOA and BBOA factors at night. Resolving by time-of-day allows the identification of different types of BBOA; the midday BBOA is associated with chloride and nighttime BBOA is associated with black carbon. In monsoon, a mixed COA-HOA factor is obtained at midday, but separate clean HOA and COA factors are obtained at night. Even the mixed COA-HOA factor shows clear markers associated with influence of heated cooking oils, especially seen in Asian cooking. Such markers are not seen in seasonal PMF. PMF analysis also separates two OOA factors in each period, one more local and the other more regional in nature. The two OOA factors show signs of mixing and are therefore not discussed in detail.

In monsoon, the seasonal PMF approach underestimates POA TS at all times of the day relative to the time-of-day PMF approach. In winter, the seasonal PMF approach underestimates POA TS at midday, but overestimates POA TS at night. Several differences also occur at key *m/z*s in POA MS extracted from the two approaches. Time-of-day PMF midday POA factors are more oxidized than the seasonal PMF POA factors, in line with the high photochemical processing at midday. Differences in nighttime POA MS profiles are small.

OOA TS show strong similarity between the two approaches. However, OOA MS show lower oxidation state at monsoon midday and winter nighttime, and higher oxidation state at monsoon nighttime and winter midday in time-of-day PMF analysis compared to the seasonal PMF analysis. Presence of semi-volatile oxidized organics at monsoon midday and winter nighttime could be attributed to semi-volatile biogenic emissions in monsoon and slow oxidation processes in winter.

Q/Qexp values of the PMF solutions are a measure of quality of fit and show a decrease of 5–30% going from seasonal PMF analysis to time-of-day PMF analysis. These improvements in *Q/Qexp* can be mapped out to specific time points and *m/z*s. In winter, improvements in *Q/Qexp* are particularly larger in specific time periods in the 4 h time windows. In monsoon, the improvements are, for the most part, independent of time. In winter, improvements in *Q/Qexp* are associated with improvements at key *m/z*s. Improvements in *Q/Qexp* for all periods are partially driven by improvements in fits at *m/z*s higher than *m/z* 80.

Application of PMF on field monitoring datasets is a powerful approach to separate the effects of contributing sources. Typically, such analysis is conducted on datasets lasting from a few weeks to a few months. However, in the last decade,

several long-term aerosol mass spectrometry deployments have occurred, and one such deployment is the Delhi Aerosol Supersite study. Long-term measurements are also conducted for regulatory-level air pollution monitoring. In the coming years, source apportionment strategies could become mainstream policy tools, and organic mass spectrometry instrumentation may obtain regulatory-grade status. Given this context, the time-of-day PMF approach combines the benefits of large datasets collected using long-term monitoring with the enhancement of time-resolving capability of source apportionment approaches such as PMF at a lower computational intensity compared to the traditional approaches. Results in this paper demonstrate that time-of-day PMF approach gives a greater number of factors as well as more representative PMF factors compared to the traditional seasonal PMF approach.

Appendix A: Abbreviations

ACSM	Aerosol Chemical Speciation Monitor
BBOA	Biomass-burning organic aerosol
BC	Black carbon
BC_{BB}	Wood burning component of BC
BC_{FF}	Fossil fuel component of BC
BS	Bootstrapping
BS-DISP	Bootstrapping enhanced with displacement
CO	Carbon monoxide
COA	Cooking organic aerosol
DAS	Delhi Aerosol Supersite
DISP	dQ-controlled displacement of factor elements
HOA	Hydrocarbon-like organic aerosol
IIT	Indian Institute of Technology
LT	Local Time
ME-2	Multilinear Engine
MS	Mass spectral profiles
NCR	National Capital Region
$NR\text{-}PM_1$	Non-refractory submicron particulate matter
$NR\text{-}PM_{2.5}$	Non-refractory PM smaller than 2.5 μm in diameter
OOA	Oxygenated organic aerosol
Org	Organic
PBLH	Planetary boundary layer height

PET	PMF evaluation tool
PM	Particulate matter
PM$_1$	Submicron particulate matter
PM$_{2.5}$	Particulate matter smaller than 2.5 μm in diameter
PMF	Positive matrix factorization
POA	Primary organic aerosol
SD	Standard deviation
SFC-OA	Solid fuel combustion organic aerosol
SOA	Secondary organic aerosol
SoFi	Source Finder
SVOOA	Semi-volatile oxygenated organic aerosol
SWR	Shortwave radiative flux
T	Temperature
TS	Time Series
UVPM	Ultraviolet-absorbing particulate matter
VBS	Volatility basis set
VC	Ventilation coefficient

Data availability

Data published in this main paper's figures and tables are available via the Texas Data Repository (https://doi.org/10.xxxxxxx, Hildebrandt Ruiz, 2022). Underlying research data are also available by request to Lea Hildebrandt Ruiz: lhr@che.utexas.edu.

670 **Author contributions**

LHR, JSA, GH, and SB designed the study. SB and ZA carried out the data collection. SB carried out the data processing and analysis. SB, JSA, and LHR assisted with the interpretation of results. All co-authors contributed to writing and reviewing the paper.

Competing interests

675 The authors declare that they have no conflict of interest.

References

Abdullahi, K. L., Delgado-Saborit, J. M., and Harrison, R. M.: Emissions and indoor concentrations of particulate matter and its specific chemical components from cooking: a review, Atmospheric Environment, 71, 260–294, URL https://doi.org/10.1016/j.atmosenv.2013.01.061, 2013.

Allan, J. D., Williams, P. I., Morgan, W. T., Martin, C. L., Flynn, M. J., Lee, J., Nemitz, E., Phillips, G. J., Gallagher, M. W., and Coe, H.: Contributions from transport, solid fuel burning and cooking to primary organic aerosols in two UK cities, Atmospheric Chemistry and Physics, 10, 647–668, URL https://acp.copernicus.org/articles/10/647/2010/, 2010.

Amato, F. and Hopke, P. K.: Source apportionment of the ambient PM2.5 across St. Louis using constrained positive matrix factorization, Atmospheric Environment, 46, 329–337, URL https://doi.org/10.1016/j.atmosenv.2011.09.062, 2012.

Amato, F., Pandolfi, M., Escrig, A., Querol, X., Alastuey, A., Pey, J., Perez, N., and Hopke, P. K.: Quantifying road dust resuspension in urban environment by Multilinear Engine: a comparison with PMF2, Atmospheric Environment, 43, 2770–2780, URL https://doi.org/10.1016/j.atmosenv.2009.02.039, 2009.

Amil, N., Latif, M. T., Khan, M. F., and Mohamad, M.: Seasonal variability of PM2.5 composition and sources in the Klang Valley urban-industrial environment, Atmospheric Chemistry and Physics, 16, 5357–5381, URL https://doi.org/10.5194/acp-16-5357-2016, 2016.

Angelis, E. D., Carnevale, C., Turrini, E., and Volta, M.: Source apportionment and integrated assessment modelling for air quality planning, Electronics, 9, URL https://www.mdpi.com/2079-9292/9/7/1098, 2020.

Arub, Z., Bhandari, S., Gani, S., Apte, J. S., Ruiz, L. H., and Habib, G.: Air mass physiochemical characteristics over New Delhi: impacts on aerosol hygroscopicity and cloud condensation nuclei (CCN) formation, Atmospheric
710   Chemistry and Physics, 20, 6953–6971, URL https://acp.copernicus.org/articles/20/6953/2020/, 2020.

Bahreini, R., Keywood, M. D., Ng, N. L., Varutbangkul, V., Gao, S., Flagan, R. C., Seinfeld, J. H., Worsnop, D. R., and Jimenez, J. L.: Measurements of secondary organic aerosol from oxidation of cycloalkenes, terpenes, and m-xylene using an aerodyne aerosol mass spectrometer, Environmental Science and Technology, 39, 5674–5688, URL https://pubs.acs.org/doi/abs/10.1021/es048061a, 2005.

715   Belis, C. A., Karagulian, F., Larsen, B. R., and Hopke, P. K.: Critical review and meta-analysis of ambient particulate matter source apportionment using receptor models in Europe, Atmospheric Environment, 69, 94–108, URL https://doi.org/10.1016/j.atmosenv.2012.11.009, 2013.

Belis, C. A., Larsen, B. R., Amato, F., Haddad, E., Favez, O., Harrison, R. M., Hopke, P. K., Nava, S., Paatero, P., Prévôt, A., Quass, U., and Vecchi, R.: European guide on air pollution source apportionment with receptor models,
720   URL   https://ec.europa.eu/jrc/en/publication/european-guide-air-pollution-source-apportionment-receptor-models, 2014.

Belis, C. A., Karagulian, F., Amato, F., Almeida, M., Artaxo, P., Beddows, D. C., Bernardoni, V., Bove, M. C., Carbone, S., Cesari, D., Contini, D., Cuccia, E., Diapouli, E., Eleftheriadis, K., Favez, O., Haddad, I. E., Harrison, R. M., Hellebust, S., Hovorka, J., Jang, E., Jorquera, H., Kammermeier, T., Karl, M., Lucarelli, F., Mooibroek, D., Nava,
725   S., Nøjgaard, J. K., Paatero, P., Pandolfi, M., Perrone, M. G., Petit, J. E., Pietrodangelo, A., Pokorná, P., Prati, P., Prevot, A. S., Quass, U., Querol, X., Saraga, D., Sciare, J., Sfetsos, A., Valli, G., Vecchi, R., Vestenius, M., Yubero, E., and Hopke, P. K.: A new methodology to assess the performance and uncertainty of source apportionment models II: the results of two European intercomparison exercises, Atmospheric Environment, 123, 240–250, URL https://doi.org/10.1016/j.atmosenv.2015.10.068, 2015.

730   Bertrand, A., Stefenelli, G., Bruns, E. A., Pieber, S. M., Temime-Roussel, B., Slowik, J. G., Prévôt, A. S., Wortham, H., Haddad, I. E., and Marchand, N.: Primary emissions and secondary aerosol production potential from woodstoves for residential heating: influence of the stove technology and combustion efficiency, Atmospheric Environment, 169, 65–79, URL https://doi.org/10.1016/j.atmosenv.2017.09.005, 2017.

Bhandari, S., Gani, S., Patel, K., Wang, D. S., Soni, P., Arub, Z., Habib, G., Apte, J. S., and Ruiz, L. H.: Sources and
735   atmospheric dynamics of organic aerosol in New Delhi, India: insights from receptor modeling, Atmospheric Chemistry and Physics, 20, 735–752, URL https://acp.copernicus.org/articles/20/735/2020/, 2020.

Bhandari, S., Arub, Z., Habib, G., Apte, J. S., and Ruiz, L. H.: Contributions of primary sources to submicron organic aerosols in Delhi, India, https://acp.copernicus.org/preprints/acp-2022-179/, submitted to Atmospheric Chemistry and Physics, 2022..

740   Bikkina, S., Andersson, A., Kirillova, E. N., Holmstrand, H., Tiwari, S., Srivastava, A. K., Bisht, D. S., and Örjan Gustafsson: Air quality in megacity Delhi affected by countryside biomass burning, Nature Sustainability, 2, 200–205, URL https://doi.org/10.1038/s41893-019-0219-0, 2019.

Brown, S. G., Lee, T., Norris, G. A., Roberts, P. T., Collett, J. L., Paatero, P., and Worsnop, D. R.: Receptor modeling of near-roadway aerosol mass spectrometer data in Las Vegas, Nevada, with EPA PMF, Atmospheric Chemistry and
745   Physics, 12, 309–325, URL https://acp.copernicus.org/articles/12/309/2012/, 2012.

Brown, S. G., Eberly, S., Paatero, P., and Norris, G. A.: Methods for estimating uncertainty in PMF solutions: examples with ambient air and water quality data and guidance on reporting PMF results, Science of the Total Environment, 518-519, 626–635, URL https://doi.org/10.1016/j.scitotenv.2015.01.022, 2015.

California Air Resources Board: AB 617 recommended source attribution technical approaches, URL
750   https://ww2.arb.ca.gov/resources/documents/ab-617-recommended-source-attribution-technical-approaches, 2018.

Canonaco, F., Crippa, M., Slowik, J. G., Baltensperger, U., and Prévôt, A. S. H.: SoFi, an IGOR based interface for the efficient use of the generalized multilinear engine (ME-2) for the source apportionment: ME-2 application to aerosol mass spectrometer data, Atmospheric Measurement Techniques, 6, 3649–3661, URL https://amt.copernicus.org/articles/6/3649/2013/, 2013.

755   Canonaco, F., Slowik, J. G., Baltensperger, U., and Prévôt, A. S. H.: Seasonal differences in oxygenated organic aerosol composition: implications for emissions sources and factor analysis, Atmospheric Chemistry and Physics, 15, 6993–7002, URL https://acp.copernicus.org/articles/15/6993/2015/, 2015.

Canonaco, F., Tobler, A., Chen, G., Sosedova, Y., Slowik, J. G., Bozzetti, C., Daellenbach, K.R., El Haddad, I., Crippa, M., Huang, R.-J., Furger, M., Baltensperger, U., and Prévôt, A. S. H.: A new method for long-term source
760   apportionment with time-dependent factor profiles and uncertainty assessment using SoFi Pro: application to one year of organic aerosol data, Atmospheric Measurement Techniques Discussions, "in press", 1–39, URL https://doi.org/10.5194/amt-2020-204, 2020.

Carslaw, D. C. and Ropkins, K.: openair: an R package for air quality data analysis, Environmental Modelling and Software, 27–28, 52–61, URL https://doi.org/10.1016/j.envsoft.2011.09.008, 2012.

765   Crippa, M., DeCarlo, P. F., Slowik, J. G., Mohr, C., Heringa, M. F., Chirico, R., Poulain, L., Freutel, F., Sciare, J., Cozic, J., Marco, C. F. D., Elsasser, M., Nicolas, J. B., Marchand, N., Abidi, E., Wiedensohler, A., Drewnick, F., Schneider, J., Borrmann, S., Nemitz, E., Zimmermann, R., Jaffrezo, J.-L., Prévôt, A. S. H., and Baltensperger, U.: Wintertime aerosol chemical composition and source apportionment of the organic fraction in the metropolitan area of Paris, Atmospheric Chemistry and Physics, 13, 961–981, URL https://acp.copernicus.org/articles/13/961/2013/,
770   2013.

Crippa, M., Canonaco, F., Lanz, V. A., Äijälä, M., Allan, J. D., Carbone, S., Capes, G., Ceburnis, D., Dall'Osto, M., Day, D. A., DeCarlo, P. F., Ehn, M., Eriksson, A., Freney, E., Ruiz, L. H., Hillamo, R., Jimenez, J. L., Junninen, H., Kiendler-Scharr, A., Kortelainen, A.-M., Kulmala, M., Laaksonen, A., Mensah, A. A., Mohr, C., Nemitz, E.,

775 O'Dowd, C., Ovadnevaite, J., Pandis, S. N., Petäjä, T., Poulain, L., Saarikoski, S., Sellegri, K., Swietlicki, E., Tiitta, P., Worsnop, D. R., Baltensperger, U., and Prévôt, A. S. H.: Organic aerosol components derived from 25 AMS data sets across Europe using a consistent ME-2 based source apportionment approach, Atmospheric Chemistry and Physics, 14, 6159–6176, URL https://acp.copernicus.org/articles/14/6159/2014/, 2014.

Crippa, M., Solazzo, E., Huang, G., Guizzardi, D., Koffi, E., Muntean, M., Schieberle, C., Friedrich, R., and Janssens-Maenhout, G.: High resolution temporal profiles in the Emissions Database for Global Atmospheric Research,
780 Scientific Data, 7, 1–17, URL https://www.nature.com/articles/s41597-020-0462-2, 2020.

Daellenbach, K. R., Uzu, G., Jiang, J., Cassagnes, L. E., Leni, Z., Vlachou, A., Stefenelli, G. Canonaco, F., Weber, S., Segers, A., Kuenen, J. J., Schaap, M., Favez, O., Albinet, A., Aksoyoglu, S., Dommen, J., Baltensperger, U., Geiser, M., Haddad, I. E., Jaffrezo, J. L., and Prévôt, A. S.: Sources of particulate-matter air pollution and its oxidative potential in Europe, Nature, 587, 414–419, URL https://doi.org/10.1038/s41586-020-2902-8, 2020.

785 Dai, Q., Liu, B., Bi, X., Wu, J., Liang, D., Zhang, Y., Feng, Y., and Hopke, P. K.: Dispersion normalized PMF provides insights into the significant changes in source contributions to PM2.5 after the CoviD-19 outbreak, Environmental Science and Technology, 54, 9917–9927, URL https://dx.doi.org/10.1021/acs.est.0c02776, 2020.

Dallmann, T. R., Onasch, T. B., Kirchstetter, T. W., Worton, D. R., Fortner, E. C., Herndon, S. C., Wood, E. C., Franklin, J. P., Worsnop, D. R., Goldstein, A. H., and Harley, R. A.: Characterization of particulate matter emissions
790 from on-road gasoline and diesel vehicles using a soot particle aerosol mass spectrometer, Atmospheric Chemistry and Physics, 14, 7585–7599, URL https://acp.copernicus.org/articles/14/7585/2014/, 2014.

Dall'Osto, M., Paglione, M., Decesari, S., Facchini, M. C., O'Dowd, C., Plass-Duellmer, C., and Harrison, R. M.: On the origin of AMS "cooking organic aerosol" at a rural site, Environmental Science and Technology, 49, 13964–13972, URL https://pubs.acs.org/doi/abs/10.1021/acs.est.5b02922, 2015.

795 Drinovec, L., Mocnik, G., Zotter, P., Prévôt, A. S., Ruckstuhl, C., Coz, E., Rupakheti, M., Sciare, J., Müller, T., Wiedensohler, A., and Hansen, A. D.: The "dual-spot" aethalometer: an improved measurement of aerosol black carbon with real-time loading compensation, Atmospheric Measurement Techniques, 8, 1965–1979, URL https://doi.org/10.5194/amt-8-1965-2015, 2015.

Drosatou, A. D., Skyllakou, K., Theodoritsi, G. N., and Pandis, S. N.: Positive matrix factorization of organic aerosol:
800 insights from a chemical transport model, Atmospheric Chemistry and Physics, 19, 973–986, URL https://acp.copernicus.org/articles/19/973/2019/, 2019.

Environmental Protection Agency: 40 CFR Part 51 Revisions to the guideline on air quality models: enhancements to the AERMOD dispersion modeling system and incorporation of approaches to address ozone and fine particulate matter, URL https://www.federalregister.gov/documents/2017/01/17/2016-31747/revisions-to-the-guideline-on-air-
805 quality-models-enhancements-to-the-aermod-dispersion-modeling, 2017.

Fourtziou, L., Liakakou, E., Stavroulas, I., Theodosi, C., Zarmpas, P., Psiloglou, B., Sciare, J., Maggos, T., Bairachtari, K., Bougiatioti, A., Gerasopoulos, E., Sarda-Estève, R., Bonnaire, N., and Mihalopoulos, N.: Multi-tracer

approach to characterize domestic wood burning in Athens (Greece) during wintertime, Atmospheric Environment, 148, 89–101, URL https://doi.org/10.1016/j.atmosenv.2016.10.011, 2017.

810   Fröhlich, R., Crenn, V., Setyan, A., Belis, C. A., Canonaco, F., Favez, O., Riffault, V., Slowik, J. G., Aas, W., Aijälä, M., Alastuey, A., Artiñano, B., Bonnaire, N., Bozzetti, C., Bressi, M., Carbone, C., Coz, E., Croteau, P. L., Cubison, M. J., Esser-Gietl, J. K., Green, D. C., Gros, V., Heikkinen, L., Herrmann, H., Jayne, J. T., Lunder, C. R., Minguillón, M. C., Mocnik, G., O'Dowd, C. D., Ovadnevaite, J., Petralia, E., Poulain, L., Priestman, M., Ripoll, A., Sarda-Estève, R., Wiedensohler, A., Baltensperger, U., Sciare, J., and Prévôt, A. S. H.: ACTRIS ACSM intercomparison–Part 2:

815   intercomparison of ME-2 organic source apportionment results from 15 individual, co-located aerosol mass spectrometers, Atmospheric Measurement Techniques, 8, 2555–2576,
        URL https://amt.copernicus.org/articles/8/2555/2015/, 2015.

        Gani, S., Bhandari, S., Patel, K., Seraj, S., Soni, P., Arub, Z., Habib, G., Ruiz, L. H., and Apte, J. S.: Particle number concentrations and size distribution in a polluted megacity: the Delhi Aerosol Supersite study, Atmospheric

820   Chemistry and Physics, 20, 8533–8549, URL https://doi.org/10.5194/acp-20-8533-2020, 2020.

        Goodkind, A. L., Tessum, C. W., Coggins, J. S., Hill, J. D., and Marshall, J. D.: Fine-scale damage estimates of particulate matter air pollution reveal opportunities for location-specific mitigation of emissions, Proceedings of the National Academy of Sciences of the United States of America, 116, 8775–8780, URL https://www.pnas.org/content/116/18/8775, 2019.

825   Grolemund, G. and Wickham, H.: Dates and times made easy with lubridate, Journal of Statistical Software, 40, 1–25, URL http://www.jstatsoft.org/v40/i03/, 2011.

        Gunantara, N. and Ai, Q.: A review of multi-objective optimization: methods and its applications, Cogent Engineering, 5, URL https://www.tandfonline.com/doi/full/10.1080/23311916.2018.1502242, 2018.

        Guttikunda, S. K. and Calori, G.: A GIS based emissions inventory at 1 km × 1 km spatial resolution for air pollution

830   analysis in Delhi, India, Atmospheric Environment, 67, 101–111,
        URL https://doi.org/10.1016/j.atmosenv.2012.10.040, 2013.

        Hajat, A., Hsia, C., and O'Neill, M. S.: Socioeconomic disparities and air pollution exposure: a global review, Current environmental health reports, 2, 440–450, URL https://link.springer.com/article/10.1007/s40572-015-0069-5, 2015.

        Hayfield, T. and Racine, J. S.: Nonparametric econometrics: the np package, Journal of Statistical Software, 27, URL

835   http://www.jstatsoft.org/v27/i05/, 2008.

        He, L.-Y., Lin, Y., Huang, X.-F., Guo, S., Xue, L., Su, Q., Hu, M., Luan, S.-J., and Zhang, Y.-H.: Characterization of high-resolution aerosol mass spectra of primary organic aerosol emissions from Chinese cooking and biomass burning, Atmospheric Chemistry and Physics, 10, 11535–11543,
        URL https://acp.copernicus.org/articles/10/11535/2010/, 2010.

840   Health Effects Institute: State of global air 2020: special report, URL https://www.stateofglobalair.org/, 2020.

Heikkinen, L., Äijälä, M., Riva, M., Luoma, K., Dällenbach, K., Aalto, J., Aalto, P., Aliaga, D., Aurela, M., Keskinen, H., Makkonen, U., Rantala, P., Kulmala, M., Petäjä, T., Worsnop, D., and Ehn, M.: Long-term sub-micrometer aerosol chemical composition in the boreal forest: inter- and intra-annual variability, Atmospheric Chemistry and Physics, 20, 3151–3180, URL https://acp.copernicus.org/articles/20/3151/2020/, 2020.

845   Hemann, J. G., Brinkman, G. L., Dutton, S. J., Hannigan, M. P., Milford, J. B., and Miller, S.L.: Assessing positive matrix factorization model fit: a new method to estimate uncertainty and bias in factor contributions at the measurement time scale, Atmospheric Chemistry and Physics, 9, 497–513,

URL https://acp.copernicus.org/articles/9/497/2009/, 2009.

Hopke, P. K.: Review of receptor modeling methods for source apportionment, Journal of the Air and Waste
850   Management Association, 66, 237–259, URL https://doi.org/10.1080/10962247.2016.1140693, 2016.

Hu, W., Hu, M., Hu, W., Jimenez, J. L., Yuan, B., Chen, W., Wang, M., Wu, Y., Chen, C., Wang, Z., Peng, J., Zeng, L., and Shao, M.: Chemical composition, sources, and aging process of submicron aerosols in Beijing: contrast between summer and winter, Journal of Geophysical Research, 121, 1955–1977,

URL https://doi.org/10.1002/2015JD024020, 2016.

855   Huang, X.-F., He, L.-Y., Hu, M., Canagaratna, M. R., Sun, Y., Zhang, Q., Zhu, T., Xue, L., Zeng, L.-W., Liu, X.-G., Zhang, Y.-H., Jayne, J. T., Ng, N. L., and Worsnop, D. R.: Highly time-resolved chemical characterization of atmospheric submicron particles during 2008 Beijing Olympic Games using an Aerodyne High-Resolution Aerosol Mass Spectrometer, Atmospheric Chemistry and Physics, 10, 8933–8945,

URL https://acp.copernicus.org/articles/10/8933/2010/, 2010.

860   Indian National Science Academy: Seasons of Delhi, URL https://www.insaindia.res.in/climate.php, 2021.

Intergovernmental Panel on Climate Change, 2019: Summary for Policymakers. In: Climate Change and Land: an IPCC special report on climate change, desertification, land degradation, sustainable land management, food security, and greenhouse gas fluxes in terrestrial ecosystems, URL https://www.ipcc.ch/srccl/chapter/summary-for-policymakers/, 2019.

865   Intergovernmental Panel on Climate Change, 2021: Summary for Policymakers. In: Climate Change 2021: The Physical Science Basis. Contribution of Working Group I to the Sixth Assessment Report of the Intergovernmental Panel on Climate Change, https://www.ipcc.ch/report/ar6/wg1/downloads/report/IPCC_AR6_WGI_SPM_final.pdf, 2021.

Jimenez, J. L., Canagaratna, M. R., Donahue, N. M., Prevot, A. S., Zhang, Q., Kroll, J. H., DeCarlo, P. F., Allan, J.
870   D., Coe, H., Ng, N. L., Aiken, A. C., Docherty, K. S., Ulbrich, I. M., Grieshop, A. P., Robinson, A. L., Duplissy, J., Smith, J. D., Wilson, K. R., Lanz, V. A., Hueglin, C., Sun, Y. L., Tian, J., Laaksonen, A., Raatikainen, T., Rautiainen, J., Vaattovaara, P., Ehn, M., Kulmala, M., Tomlinson, J. M., Collins, D. R., Cubison, M. J., Dunlea, E. J., Huffman, J. A., Onasch, T. B., Alfarra, M. R., Williams, P. I., Bower, K., Kondo, Y., Schneider, J., Drewnick, F., Borrmann, S., Weimer, S., Demerjian, K., Salcedo, D., Cottrell, L., Griffin, R., Takami, A., Miyoshi, T., Hatakeyama, S.,

875   Shimono, A., Sun, J. Y., Zhang, Y. M., Dzepina, K., Kimmel, J. R., Sueper, D., Jayne, J. T., Herndon, S. C., Trimborn, A. M., Williams, L. R., Wood, E. C., Middlebrook, A. M., Kolb, C. E., Baltensperger, U., and Worsnop, D. R.: Evolution of organic aerosols in the atmosphere, Science, 326, 1525–1529,

URL https://science.sciencemag.org/content/326/5959/1525, 2009.

       Khare, P., Machesky, J., Soto, R., He, M., Presto, A. A., and Gentner, D. R.: Asphalt-related emissions are a major
880   missing nontraditional source of secondary organic aerosol precursors, Science Advances, 6,

URL https://doi.org/10.1126/sciadv.abb9785, 2020.

       Kumar, S., Aggarwal, S. G., Gupta, P. K., and Kawamura, K.: Investigation of the tracers for plastic-enriched waste burning aerosols, Atmospheric Environment, 108, 49–58,

URL https://doi.org/10.1016/j.atmosenv.2015.02.066, 2015.

885   Lei, R., Feng, S., and Lauvaux, T.: Country-scale trends in air pollution and fossil fuel CO2 emissions during 2001-2018: confronting the roles of national policies and economic growth, Environmental Research Letters, 16,

URL https://doi.org/10.1088/1748-9326/abc9e1, 2021.

       Lelieveld, J. and Crutzen, P. J.: The role of clouds in tropospheric photochemistry, Journal of Atmospheric Chemistry, 12, 229–267, URL https://link.springer.com/article/10.1007/BF00048075, 1991.

890   Li, J., Song, Y., Mao, Y., Mao, Z., Wu, Y., Li, M., Huang, X., He, Q., and Hu, M.: Chemical characteristics and source apportionment of PM2.5 during the harvest season in eastern China's agricultural regions, Atmospheric Environment, 92, 442–448, URL https://doi.org/10.1016/j.atmosenv.2014.04.058, 2014a.

       Li, J., Wang, G., Aggarwal, S. G., Huang, Y., Ren, Y., Zhou, B., Singh, K., Gupta, P. K., Cao, J., and Zhang, R.: Comparison of abundances, compositions and sources of elements, inorganic ions and organic compounds in
895   atmospheric aerosols from Xi'an and New Delhi, two megacities in China and India, Science of the Total Environment, 476-477, 485–495, URL https://doi.org/10.1016/j.scitotenv.2014.01.011, 2014b.

       Lin, C., Ceburnis, D., Hellebust, S., Buckley, P., Wenger, J., Canonaco, F., Prévôt, A. S. H., Huang, R. J., O'Dowd, C., and Ovadnevaite, J.: Characterization of primary organic aerosol from domestic wood, peat, and coal burning in Ireland, Environmental Science and Technology, 51, 10624–10632,

900 URL https://doi.org/10.1021/acs.est.7b01926, 2017.

       Liu, Q., Sun, Y., Hu, B., Liu, Z. R., Akio, S., and Wang, Y. S.: In situ measurement of PM1 organic aerosol in Beijing winter using a high-resolution aerosol mass spectrometer, Chinese Science Bulletin, 57, 819–826,

URL https://doi.org/10.1007/s11434-011-4886-0, 2012.

       Liu, T., Wang, Z., Wang, X., and Chan, C. K.: Primary and secondary organic aerosol from heated cooking oil
905   emissions, Atmospheric Chemistry and Physics, 18, 11363–11374,

URL https://acp.copernicus.org/articles/18/11363/2018/, 2018.

       Lu, J. G.: Air pollution: a systematic review of its psychological, economic, and social effects, Current Opinion in Psychology, 32, 52–65, URL https://doi.org/10.1016/j.copsyc.2019.06.024, 2020.

Mishra, R. K., Pandey, A., Pandey, G., and Kumar, A.: The effect of odd-even driving scheme on PM2.5 and PM1.0 emission, Transportation Research Part D: Transport and Environment, 67, 541–552, URL https://doi.org/10.1016/j.trd.2019.01.005, 2019.

Misra, P., Imasu, R., Hayashida, S., Arbain, A. A., Avtar, R., and Takeuchi, W.: Mapping brick kilns to support environmental impact studies around Delhi using Sentinel-2, ISPRS International Journal of Geo-Information, 9, URL https://www.mdpi.com/2220-9964/9/9/544, 2020.

Ng, N. L., Canagaratna, M. R., Zhang, Q., Jimenez, J. L., Tian, J., Ulbrich, I. M., Kroll, J. H., Docherty, K. S., Chhabra, P. S., Bahreini, R., Murphy, S. M., Seinfeld, J. H., Hildebrandt, L., Donahue, N. M., DeCarlo, P. F., Lanz, V. A., Prévôt, A. S. H., Dinar, E., Rudich, Y., and Worsnop, D. R.: Organic aerosol components observed in northern hemispheric datasets from aerosol mass spectrometry, Atmospheric Chemistry and Physics, 10, 4625–4641, URL https://acp.copernicus.org/articles/10/4625/2010/, 2010.

Ng, N. L., Canagaratna, M. R., Jimenez, J. L., Zhang, Q., Ulbrich, I. M., and Worsnop, D. R.: Realtime methods for estimating organic component mass concentrations from aerosol mass spectrometer data, Environmental Science and Technology, 45, 910–916, URL https://pubs.acs.org/doi/abs/10.1021/es102951k, 2011a.

Ng, N. L., Herndon, S. C., Trimborn, A., Canagaratna, M. R., Croteau, P. L., Onasch, T. B., Sueper, D., Worsnop, D. R., Zhang, Q., Sun, Y. L., and Jayne, J. T.: An Aerosol Chemical Speciation Monitor (ACSM) for routine monitoring of the composition and mass concentrations of ambient aerosol, Aerosol Science and Technology, 45, 780–794, URL http://www.tandfonline.com/doi/abs/10.1080/02786826.2011.560211, 2011b.

Norris, G., Duvall, R., Brown, S., and Bai, S.: EPA Positive Matrix Factorization 5.0 fundamentals and user guide, URL https://www.epa.gov/air-research/epa-positive-matrix-factorization-50-fundamentals-and-user-guide, 2014.

Olson, M. R., Garcia, M. V., Robinson, M. A., Rooy, P. V., Dietenberger, M. A., Bergin, M., and Schauer, J. J.: Investigation of black and brown carbon multiple-wavelength dependent light absorption from biomass and fossil fuel combustion source emissions, Journal of Geophysical Research, 120, 6682–6697, URL https://doi.org/10.1002/2014JD022970, 2015.

Organization for Economic Co-operation and Development: The economic cost of air pollution: evidence from Europe, URL https://www.oecd-ilibrary.org/economics/the-economic-cost-of-air-pollution-evidence-from-europe_56119490-en, 2020.

Paatero, P.: Least squares formulation of robust non-negative factor analysis, Chemometrics and Intelligent Laboratory Systems, 37, 23–35, URL https://doi.org/10.1016/S0169-7439(96)00044-5, 1997.

Paatero, P.: The Multilinear Engine—a table-driven, least squares program for solving multilinear problems, including the n-way parallel factor analysis model, Journal of Computational and Graphical Statistics, 8, 854–888, URL https://www.tandfonline.com/doi/abs/10.1080/10618600.1999.10474853, 1999.

Paatero, P. and Hopke, P. K.: Discarding or downweighting high-noise variables in factor analytic models, Analytica Chimica Acta, 490, 277–289, URL https://doi.org/10.1016/S0003-2670(02)01643-4, 2003.

Paatero, P. and Hopke, P. K.: Rotational tools for factor analytic models, Journal of Chemometrics, 23, 91–100, URL http://doi.wiley.com/10.1002/cem.1197, 2009.

945   Paatero, P. and Tapper, U.: Positive matrix factorization: a non-negative factor model with optimal utilization of error estimates of data values, Environmetrics, 5, 111–126, URL https://doi.org/10.1002/env.3170050203, 1994.

Paatero, P., Hopke, P. K., Song, X. H., and Ramadan, Z.: Understanding and controlling rotations in factor analytic models, Chemometrics and Intelligent Laboratory Systems, 60, 253–264,

URL https://doi.org/10.1016/S0169-7439(01)00200-3, 2002.

950   Paatero, P., Eberly, S., Brown, S. G., and Norris, G. A.: Methods for estimating uncertainty in factor analytic solutions, Atmospheric Measurement Techniques, 7, 781–797, URL https://amt.copernicus.org/articles/7/781/2014/, 2014.

Pandey, A., Brauer, M., Cropper, M. L., Balakrishnan, K., Mathur, P., Dey, S., Turkgulu, B., Kumar, G. A., Khare, M., Beig, G., Gupta, T., Krishnankutty, R. P., Causey, K., Cohen, A. J., Bhargava, S., Aggarwal, A. N., Agrawal, A.,

955   Awasthi, S., Bennitt, F., Bhagwat, S., Bhanumati, P., Burkart, K., Chakma, J. K., Chiles, T. C., Chowdhury, S., Christopher, D. J., Dey, S., Fisher, S., Fraumeni, B., Fuller, R., Ghoshal, A. G., Golechha, M. J., Gupta, P. C., Gupta, R., Gupta, R., Gupta, S., Guttikunda, S., Hanrahan, D., Harikrishnan, S., Jeemon, P., Joshi, T. K., Kant, R., Kant, S., Kaur, T., Koul, P. A., Kumar, P., Kumar, R., Larson, S. L., Lodha, R., Madhipatla, K. K., Mahesh, P. A., Malhotra, R., Managi, S., Martin, K., Mathai, M., Mathew, J. L., Mehrotra, R., Mohan, B. V. M., Mohan, V., Mukhopadhyay,

960   S., Mutreja, P., Naik, N., Nair, S., Pandian, J. D., Pant, P., Perianayagam, A., Prabhakaran, D., Prabhakaran, P., Rath, G. K., Ravi, S., Roy, A., Sabde, Y. D., Salvi, S., Sambandam, S., Sharma, B., Sharma, M., Sharma, S., Sharma, R. S., Shrivastava, A., Singh, S., Singh, V., Smith, R., Stanaway, J. D., Taghian, G., Tandon, N., Thakur, J. S., Thomas, N. J., Toteja, G. S., Varghese, C. M., Venkataraman, C., Venugopal, K. N., Walker, K. D., Watson, A. Y., Wozniak, S., Xavier, D., Yadama, G. N., Yadav, G., Shukla, D. K., Bekedam, H. J., Reddy, K. S., Guleria, R., Vos, T., Lim, S.

965   S., Dandona, R., Kumar, S., Kumar, P., Landrigan, P. J., and Dandona, L.: Health and economic impact of air pollution in the states of India: the Global Burden of Disease Study 2019, The Lancet Planetary Health, 5, 25–38, URL https://doi.org/10.1016/S2542-5196(20)30298-9, 2020.

Park, M. B., Lee, T. J., Lee, E. S., and Kim, D. S.: Enhancing source identification of hourly PM2.5 data in Seoul based on a dataset segmentation scheme by positive matrix factorization (PMF), Atmospheric Pollution Research, 10,

970   1042–1059, URL https://doi.org/10.1016/j.apr.2019.01.013, 2019.

Patel, K., Bhandari, S., Gani, S., Campmier, M. J., Kumar, P., Habib, G., Apte, J., and Ruiz, L. H.: Sources and dynamics of submicron aerosol during the Autumn onset of the air pollution season in Delhi, India, ACS Earth and Space Chemistry, URL https://pubs.acs.org/doi/10.1021/acsearthspacechem.0c00340, 2021a.

Patel, K., Campmier, M.J., Bhandari, S., Baig, N., Gani, S., Habib, G., Apte, J.S. and Hildebrandt Ruiz, L., 2021.

975   Persistence of Primary and Secondary Pollutants in Delhi: Concentrations and Composition from 2017 through the COVID Pandemic. Environmental Science & Technology Letters, 8, 7, 492–497,

URL https://doi.org/10.1021/acs.estlett.1c00211, 2021b.

Patel, S., Sankhyan, S., Boedicker, E. K., Decarlo, P. F., Farmer, D. K., Goldstein, A. H., Katz, E. F., Nazaroff, W. W., Tian, Y., Vanhanen, J., and Vance, M. E.: Indoor particulate matter during HOMEChem: concentrations, size distributions, and exposures, Environmental Science and Technology, 54, 7107–7116, URL https://dx.doi.org/10.1021/acs.est.0c00740, 2020.

Patton, A., Politis, D. N., and White, H.: Correction to automatic block-length selection for the dependent bootstrap by D. Politis and H. White, Econometric Reviews, 28, 372–375, URL https://doi.org/10.1080/07474930802459016, 2009.

Pauraite, J., Pivoras, A., Plauškaite, K., Bycenkiene, S., Mordas, G., Augustaitis, A., Marozas, V., Mozgeris, G., Baumgarten, M., Matyssek, R., and Ulevicius, V.: Characterization of aerosol mass spectra responses to temperature over a forest site in Lithuania, Journal of Aerosol Science, 133, 56–65, URL https://doi.org/10.1016/j.jaerosci.2019.03.010, 2019.

Politis, D. N. and White, H.: Automatic block-length selection for the dependent bootstrap, Econometric Reviews, 23, 53–70, URL https://www.tandfonline.com/doi/abs/10.1081/ETC-120028836, 2004.

R Core Team: R: a language and environment for statistical computing, R Foundation for Statistical Computing, Vienna, Austria, URL https://www.R-project.org/, 2019.

Rai, P., Furger, M., Slowik, J. G., Canonaco, F., Fröhlich, R., Hüglin, C., Minguillón, M. C., Petterson, K., Baltensperger, U., and Prévôt, A. S.: Source apportionment of highly time resolved elements during a firework episode from a rural freeway site in Switzerland, Atmospheric Chemistry and Physics, 20, 1657–1674, URL https://doi.org/10.5194/acp-20-1657-2020, 2020.

Ramadan, Z., Eickhout, B., Song, X. H., Buydens, L. M., and Hopke, P. K.: Comparison of Positive Matrix Factorization and Multilinear Engine for the source apportionment of particulate pollutants, Chemometrics and Intelligent Laboratory Systems, 66, 15–28, URL https://doi.org/10.1016/S0169-7439(02)00160-0, 2003.

Reyes-Villegas, E., Green, D. C., Priestman, M., Canonaco, F., Coe, H., Prévôt, A. S. H., and Allan, J. D.: Organic aerosol source apportionment in London 2013 with ME-2: exploring the solution space with annual and seasonal analysis, Atmospheric Chemistry and Physics, 16, 15545–15559, URL https://acp.copernicus.org/articles/16/15545/2016/, 2016.

Reyes-Villegas, E., Priestley, M., Ting, Y.-C., Haslett, S., Bannan, T., Breton, M. L., Williams, P. I., Bacak, A., Flynn, M. J., Coe, H., Percival, C., and Allan, J. D.: Simultaneous aerosol mass spectrometry and chemical ionisation mass spectrometry measurements during a biomass burning event in the UK: insights into nitrate chemistry, Atmospheric Chemistry and Physics, 18, 4093–4111, URL https://acp.copernicus.org/articles/18/4093/2018/, 2018.

Robinson, E. S., Gu, P., Ye, Q., Li, H. Z., Shah, R. U., Apte, J. S., Robinson, A. L., and Presto, A. A.: Restaurant impacts on outdoor air quality: elevated organic aerosol mass from restaurant cooking with neighborhood-scale plume extents, Environmental Science and Technology, 52, 9285–9294,

URL https://pubs.acs.org/doi/abs/10.1021/acs.est.8b02654, 2018.

Sandradewi, J., Prévôt, A. S., Szidat, S., Perron, N., Alfarra, M. R., Lanz, V. A., Weingartner, E., and Baltensperger, U. R.: Using aerosol light abosrption measurements for the quantitative determination of wood burning and traffic emission contribution to particulate matter, Environmental Science and Technology, 42, 3316–3323,

1015 URL https://doi.org/10.1021/es702253m, 2008.

Schlag, P., Kiendler-Scharr, A., Blom, M. J., Canonaco, F., Henzing, J. S., Moerman, M., Prévôt, A. S. H., and Holzinger, R.: Aerosol source apportionment from 1-year measurements at the CESAR tower in Cabauw, the Netherlands, Atmospheric Chemistry and Physics, 16, 8831–8847,

URL https://acp.copernicus.org/articles/16/8831/2016/, 2016.

1020 Schneider, J., Weimer, S., Drewnick, F., Borrmann, S., Helas, G., Gwaze, P., Schmid, O., Andreae, M. O., and Kirchner, U.: Mass spectrometric analysis and aerodynamic properties of various types of combustion-related aerosol particles, International Journal of Mass Spectrometry, 258, 37–49,

URL https://doi.org/10.1016/j.ijms.2006.07.008, 2006.

Schraufnagel, D. E., Balmes, J. R., Cowl, C. T., Matteis, S. D., Jung, S. H., Mortimer, K., Perez Padilla, R., Rice, M.
1025 B., Riojas-Rodriguez, H., Sood, A., Thurston, G. D., To, T., Vanker, A., and Wuebbles, D. J.: Air pollution and noncommunicable diseases: a review by the Forum of International Respiratory Societies' Environmental Committee, part 1: the damaging effects of air pollution, Chest, 155, 409–416,

URL https://doi.org/10.1016/j.chest.2018.10.042, 2019.

Shaddick, G., Thomas, M. L., Mudu, P., Ruggeri, G., and Gumy, S.: Half the world's population are exposed to
1030 increasing air pollution, npj Climate and Atmospheric Science, 3, 1–5, URL https://doi.org/10.1038/s41612-020-0124-2, 2020.

Stavroulas, I., Bougiatioti, A., Grivas, G., Paraskevopoulou, D., Tsagkaraki, M., Zarmpas, P., Liakakou, E., Gerasopoulos, E., and Mihalopoulos, N.: Sources and processes that control the submicron organic aerosol composition in an urban Mediterranean environment (Athens): a high temporal-resolution chemical composition
1035 measurement study, Atmospheric Chemistry and Physics, 19, 901–919,

URL https://acp.copernicus.org/articles/19/901/2019/, 2019.

Sun, Y.-L., Zhang, Q., Schwab, J. J., Demerjian, K. L., Chen, W.-N., Bae, M.-S., Hung, H.-M., Hogrefe, O., Frank, B., Rattigan, O. V., and Lin, Y.-C.: Characterization of the sources and processes of organic and inorganic aerosols in New York city with a high-resolution time-of flight aerosol mass spectrometer, Atmospheric Chemistry and
1040 Physics, 11, 1581–1602, URL https://acp.copernicus.org/articles/11/1581/2011/, 2011.

Sun, Y. L., Wang, Z. F., Fu, P. Q., Yang, T., Jiang, Q., Dong, H. B., Li, J., and Jia, J. J.: Aerosol composition, sources and processes during wintertime in Beijing, China, Atmospheric Chemistry and Physics, 13, 4577–4592,

URL https://acp.copernicus.org/articles/13/4577/2013/, 2013.

1045 Tessum, C. W., Apte, J. S., Goodkind, A. L., Muller, N. Z., Mullins, K. A., Paolella, D. A., Polasky, S., Springer, N. P., Thakrar, S. K., Marshall, J. D., and Hill, J. D.: Inequity in consumption of goods and services adds to racial-ethnic disparities in air pollution exposure, Proceedings of the National Academy of Sciences of the United States of America, 116, 6001–6006, URL https://doi.org/10.1073/pnas.1818859116, 2019.

Thakrar, S. K., Balasubramanian, S., Adams, P. J., Azevedo, I. M., Muller, N. Z., Pandis, S. N., Polasky, S., Pope, C. A., Robinson, A. L., Apte, J. S., Tessum, C. W., Marshall, J. D., and Hill, J. D.: Reducing mortality from air pollution 1050 in the United States by targeting specific emission sources, Environmental Science and Technology Letters, 7, 639–645, URL https://doi.org/10.1021/acs.estlett.0c00424, 2020.

Thamban, N. M., Tripathi, S. N., Moosakutty, S. P., Kuntamukkala, P., and Kanawade, V. P.: Internally mixed black carbon in the Indo-Gangetic Plain and its effect on absorption enhancement, Atmospheric Research, 197, 211–223, URL https://doi.org/10.1016/j.atmosres.2017.07.007, 2017.

1055 Thind, M. P., Tessum, C. W., Azevedo, I. L., and Marshall, J. D.: Fine particulate air pollution from electricity generation in the US: health impacts by race, income, and geography, Environmental Science and Technology, 53, 14010–14019, URL https://pubs.acs.org/doi/abs/10.1021/acs.est.9b02527, 2019.

Tian, J., Wang, Q., Ni, H., Wang, M., Zhou, Y., Han, Y., Shen, Z., Pongpiachan, S., Zhang, N., Zhao, Z., Zhang, Q., Zhang, Y., Long, X., and Cao, J.: Emission characteristics of primary brown carbon absorption from biomass and 1060 coal burning: development of an optical emission inventory for China, Journal of Geophysical Research: Atmospheres, 124, URL https://onlinelibrary.wiley.com/doi/abs/10.1029/2018JD029352, 2019.

Tian, Y., Xiao, Z., Wang, H., Peng, X., Guan, L., Huangfu, Y., Shi, G., Chen, K., Bi, X., and Feng, Y.: Influence of the sampling period and time resolution on the PM source apportionment: study based on the high time-resolution data and long-term daily data, Atmospheric Environment, 165, 301–309, 1065 URL https://doi.org/10.1016/j.atmosenv.2017.07.003, 2017.

Tobler, A., Bhattu, D., Canonaco, F., Lalchandani, V., Shukla, A., Thamban, N. M., Mishra, S., Srivastava, A. K., Bisht, D. S., Tiwari, S., Singh, S., Mocnik, G., Baltensperger, U., Tripathi, S. N., Slowik, J. G., and Prévôt, A. S.: Chemical characterization of PM2.5 and source apportionment of organic aerosol in New Delhi, India, Science of the Total Environment, 745, URL https://doi.org/10.1016/j.scitotenv.2020.140924, 2020.

1070 Tschofen, P., Azevedo, I. L., and Muller, N. Z.: Fine particulate matter damages and value added in the US economy, Proceedings of the National Academy of Sciences of the United States of America, 116, 19857–19862, URL www.pnas.org/cgi/doi/10.1073/pnas.1905030116, 2019.

Ulbrich, I. M., Canagaratna, M. R., Zhang, Q., Worsnop, D. R., and Jimenez, J. L.: Interpretation of organic components from Positive Matrix Factorization of aerosol mass spectrometric data, Atmospheric Chemistry and 1075 Physics, 9, 2891–2918, URL https://acp.copernicus.org/articles/9/2891/2009/, 2009.

Ulbrich, I. M., Handschy, A., Lechner, M., and Jimenez, J.: AMS Spectral Database, URL http://cires.colorado.edu/jimenez-group/AMSsd/ (last access: 25 April 2019), 2017.

Ulbrich, I. M., Handschy, A., Lechner, M., and Jimenez, J.: High-Resolution AMS Spectral Database, URL http://cires.colorado.edu/jimenez-group/HRAMSsd/ (last access: 25 April 2019), 2018.

1080   Venables, W. N. and Ripley, B. D.: Modern applied statistics with S, Springer, New York, fourth edn., URL http://www.stats.ox.ac.uk/pub/MASS4, 2002.

Venturini, E., Vassura, I., Raffo, S., Ferroni, L., Bernardi, E., and Passarini, F.: Source apportionment and location by selective wind sampling and Positive Matrix Factorization, Environmental Science and Pollution Research, 21, 11634–11648, URL https://link.springer.com/article/10.1007/s11356-014-2507-6, 2014.

1085   Wang, Q., Qiao, L., Zhou, M., Zhu, S., Griffith, S., Li, L., and Yu, J. Z.: Source apportionment of PM2.5 using hourly measurements of elemental tracers and major constituents in an urban environment: investigation of time-resolution influence, Journal of Geophysical Research: Atmospheres, 123, 5284–5300,
URL http://doi.wiley.com/10.1029/2017JD027877, 2018.

Wang, Y., Hopke, P. K., Rattigan, O. V., Xia, X., Chalupa, D. C., and Utell, M. J.: Characterization of residential
1090   wood combustion particles using the two-wavelength aethalometer, Environmental Science and Technology, 45, 7387–7393, URL https://doi.org/10.1021/es2013984, 2011.

Wayland, R. A.: EPA modeling guidance for demonstrating attainment of air quality goals for ozone, PM2.5, and regional haze, URL https://www.epa.gov/scram/state-implementation-plan-sip-attainment-demonstration-guidance., 2018.

1095   Wickham, H., Averick, M., Bryan, J., Chang, W., McGowan, L. D., François, R., Grolemund, G., Hayes, A., Henry, L., Hester, J., Kuhn, M., Pedersen, T. L., Miller, E., Bache, S. M., Müller, K., Ooms, J., Robinson, D., Seidel, D. P., Spinu, V., Takahashi, K., Vaughan, D., Wilke, C., Woo, K., and Yutani, H.: Welcome to the tidyverse, Journal of Open Source Software, 4, URL https://joss.theoj.org/papers/10.21105/joss.01686, 2019.

Williams, B. J., Goldstein, A. H., Kreisberg, N. M., Hering, S. V., Worsnop, D. R., Ulbrich, I. M., Docherty, K. S.,
1100   and Jimenez, J. L.: Major components of atmospheric organic aerosol in southern California as determined by hourly measurements of source marker compounds, Atmospheric Chemistry and Physics, 10, 11577–11603,
URL https://acp.copernicus.org/articles/10/11577/2010/, 2010.

World Health Organization: Ambient air pollution: a global assessment of exposure and burden of disease, URL https://www.who.int/phe/publications/air-pollution-global-assessment/en/, 2018.

1105   Xie, M., Barsanti, K. C., Hannigan, M. P., Dutton, S. J., and Vedal, S.: Positive matrix factorization of PM2.5-eliminating the effects of gas/particle partitioning of semivolatile organic compounds, Atmospheric Chemistry and Physics, 13, 7381–7393, URL https://doi.org/10.5194/acp-13-7381-2013, 2013a.

Xie, M., Piedrahita, R., Dutton, S. J., Milford, J. B., Hemann, J. G., Peel, J. L., Miller, S. L., Kim, S. Y., Vedal, S., Sheppard, L., and Hannigan, M. P.: Positive matrix factorization of a 32-month series of daily PM2.5 speciation data
1110   with incorporation of temperature stratification, Atmospheric Environment, 65, 11–20,
URL https://doi.org/10.1016/j.atmosenv.2012.09.034, 2013b.

Zhang, K. and Batterman, S.: Air pollution and health risks due to vehicle traffic, Science of the Total Environment, 450-451, 307–316, URL https://doi.org/10.1016/j.scitotenv.2013.01.074, 2013.

Zhang, Q., Alfarra, M. R., Worsnop, D. R., Allan, J. D., Coe, H., Canagaratna, M. R., and Jimenez, J. L.:
1115   Deconvolution and quantification of hydrocarbon-like and oxygenated organic aerosols based on aerosol mass spectrometry, Environmental Science and Technology, 39, 4938–4952,

URL https://pubs.acs.org/doi/abs/10.1021/es048568l, 2005.

Zhang, Q., Jimenez, J. L., Canagaratna, M. R., Ulbrich, I. M., Ng, N. L., Worsnop, D. R., and Sun, Y.: Understanding atmospheric organic aerosols via factor analysis of aerosol mass spectrometry: a review, Analytical and Bioanalytical
1120   Chemistry, 401, 3045–3067, URL https://link.springer.com/article/10.1007/s00216-011-5355-y, 2011.

Zhang, Y., Favez, O., Petit, J.-E., Canonaco, F., Truong, F., Bonnaire, N., Crenn, V., Amodeo, T., Prévôt, A. S. H., Sciare, J., Gros, V., and Albinet, A.: Six-year source apportionment of submicron organic aerosols from near-continuous highly time-resolved measurements at SIRTA (Paris area, France), Atmospheric Chemistry and Physics, 19, 14755–14776, URL https://acp.copernicus.org/articles/19/14755/2019/, 2019.

1125   Zhang, Z., Zhu, W., Hu, M., Wang, H., Chen, Z., Shen, R., Yu, Y., Tan, R., and Guo, S.: Secondary organic aerosol from typical Chinese domestic cooking emissions, Environmental Science and Technology Letters,

URL https://pubs.acs.org/doi/abs/10.1021/acs.estlett.0c00754, 2020.

Zheng, Y., Cheng, X., Liao, K., Li, Y., Li, Y. J., Huang, R.-J., Hu, W., Liu, Y., Zhu, T., Chen, S., Zeng, L., Worsnop, D. R., and Chen, Q.: Characterization of anthropogenic organic aerosols by TOF-ACSM with the new capture
1130   vaporizer, Atmospheric Measurement Techniques, 13, 2457–2472,

URL https://amt.copernicus.org/articles/13/2457/2020/, 2020.

Zhu, Q., Huang, X.-F., Cao, L.-M., Wei, L.-T., Zhang, B., He, L.-Y., Elser, M., Canonaco, F., Slowik, J. G., Bozzetti, C., El-Haddad, I., and Prévôt, A. S. H.: Improved source apportionment of organic aerosols in complex urban air pollution using the multilinear engine (ME-2), Atmospheric Measurement Techniques, 11, 1049–1060,
1135 URL https://amt.copernicus.org/articles/11/1049/2018/, 2018.